Feasibility Study of Battery Cooling System based on M-Cycle Evaporative Cooling

申, 嘉祺
九州大学総合理工学府総合理工学専攻機械・システム理工学メジャー

2023

Master Thesis

Feasibility Study of Battery Cooling System based on M-Cycle Evaporative Cooling

Interdisciplinary Graduate School of Engineering Sciences

Kyushu University

Department of Energy and Environmental Engineering

Thermal Energy Conversion System Laboratory

Shen JiaQi

Supervisor **Pro. Takahiko Miyazaki**

Accoc. Prof. Kyaw Thu

Submit date 2023/02/07

content

ABSTRACT **1**

Nomenclature **3**

Chapter 1: Introduction **5**

1.1 Advantages of evaporative cooling system 7

1.2 Working principle of evaporative cooling system 8

1.3 M-cycle 11

1.4 On the selection reason of M-cycle counterflow device 13

1.5 Ternary lithium battery 14

1.6 Blade battery 16

1.7 Soft-pack batteries 18

Chapter 2: Construction of Cooling System Based on M-cycle **21**

2.1 The new M-cycle system 21

2.2 Arrangement of batteries 22

2.3 Some supplementary data of M-cycle cooling box. 25

Chapter 3: Mathematical model of M-cycle cooling box **27**

3.1 The heat transferred to the air by the battery in the dry channel. 27

3.2 Heat transfer in wet channel 30

Chapter 4: Simulation result analysis **33**

4.1 On the simulation results of the cycle.（Air cooling cycle） 33

4.2 Influence of changing the channel height on the system. (air cooling system) 35

4.3 Influence of wind speed change on system refrigeration (air cooling system).....36

4.4 Influence of changing battery discharge current on system refrigeration (air cooling system).....37

4.5 Simulation result analysis (M-cycle) 39

Chapter 5： conclusion.....42

Chapter 6： For the shortcomings of this study and the possible direction of future research.....44

6.1 The shortcomings of this study 44

6.2 possibility for in-depth optimization of closed M-cycle cooling system. 44

References 46

Acknowledgement.....53

Appendix A.....54

Appendix B.....55

Feasibility Study of Battery Cooling System based on M-Cycle Evaporative Cooling

ABSTRACT

The purpose of this study is to explore whether M-cycle, as an evaporative cooling system, can stabilize the temperature of the battery within a certain range and make it not fail. The working temperature of the specific reference vehicle power battery is 20-52 degrees Celsius. In this paper, according to the traditional M-cycle semi-open circulating cooling system, a new version of M-cycle cooling cycle of closed system is proposed. And the single power battery is placed in the circulating dry channel for cooling. And detailed model concepts and related calculation formulas. Through MATLAB simulation, the relevant conclusions are finally drawn.

This study can be divided into five chapters, one is the introduction of research background. Second, the list of research objects, selection and reasons for selection. Third, a new closed evaporative cooling cycle M-cycle is proposed, and the related heat transfer relationship and calculation formula are proposed. Fourthly, the simulation results of MATLAB are analyzed and summarized. Fifth, the future direction of research is prospected and predicted.

The simulation results show that in the case of single battery, M-cycle can complete the task of temperature control of battery.

The discharge current of the battery is changed by controlling the variable method. Changing the height of the dry channel allows more air to enter the channel. Change the wind speed in the system and speed up the circulation. Three ways to test its influence on system cooling. The results show that strengthening the wind speed, expanding the height of the dry channel and reducing the discharge current of the battery as much as possible can increase the cooling efficiency of the system and reduce the battery temperature. At the same time, through the analysis of the results, it can be seen that expanding the air flow height in the main channel and accelerating the wind velocity in the system are not the bigger the better, but there is a profit peak. According to the simulation results, when the wind speed is more than 10m/s and the height of the main channel is more than 8mm, the cooling effect of the system will be improved at an inflection point, and the improvement range will be small in the later stage.

Finally, the future research direction is prospected, and several methods are put forward to improve the closed M-cycle cycle.

Key words：Evaporative cooling, Closed M-cycle, Blade battery, Battery working current, Wind speed, Dry channel height, Simulate

Nomenclature

Symbols

Tb	Battery temperature
Tb0	Initial battery temperature
∅	The calorific value of the battery per unit time
t	Battery working time
h	heat transfer coefficient
λ	thermal conductivity
l	Battery length
Nu	Nusselt Number
Pr	Prandtl Number
Re	Reynolds number
V	air velocity
v	Aerodynamic viscosity
Te	Air inlet temperature
A	Heat transfer surface area
T	Temperature
m	Mass
Cb	Battery specific heat capacity
Tdin	Inlet air temperature
λ	Thermal conductivity of battery
Nu	Nusselt Number
Re	Reynolds number
Pr	Prandtl Number
V	wind speed
v	Aerodynamic viscosity
Hw	Wet channel height
D	Channel width
ρ	air density
h''	Enthalpy of steam
h	Enthalpy of liquid water
d'	Moisture channel at outlet of wet channel

d	Moisture channel at inlet of wet channel
Tdout	Dry channel outlet temperature
Ca	Air specific heat capacity

Chapter 1: Introduction

In this chapter, the research background and research object will be elaborated in detail. The advantages of evaporative cooling cycle compared with traditional cooling mode and the advantages of M-cycle will be discussed. At the same time, the selection of the current mainstream electric vehicle power battery will also be discussed in detail. Finally, the reasons for choosing M-cycle and blade battery as the research objects will be given.

Since the industrial revolution began in Britain in the 18th century and spread to the whole world, a series of technological revolutions have caused a great leap from manual labor to power machine production. A large number of machines, mainly steam engines and internal combustion engines, began to enter people's daily lives in large numbers. Today, machines still occupy an important position in human society. But at the same time, with the vigorous development of industry, environmental problems have become a new challenge for mankind. Among them, famous events caused by environmental pollution, such as photochemical smog in Los Angeles, pollution incident in London, and Fog and Haze in China, etc. In order to solve the problem of environmental pollution, the world put forward the concept of carbon neutrality and began to transform or replace a large number of existing industrial machines that caused great pollution to the surrounding environment.

Among all kinds of pollution sources in the city, automobile exhaust emissions account for a large part, which is largely due to the extensive use of internal combustion engines. Since the 2010 Shanghai World Expo, people have been thinking about vigorously developing clean energy for industrial transformation and upgrading. Among them, electric vehicles are the concentrated embodiment of people's development in this period. In recent years, the new energy vehicles led by Tesla and BYD have a large market share in the automobile industry, and the

concept of environmental protection has become more and more popular.

Just as the core of a traditional fuel vehicle is an engine, the core of an electric vehicle is of course a power battery pack. At present, there are mainly several aspects that affect the power battery.

The first is the energy density inside the battery. According to the existing papers, the greater the density inside the battery, the higher the battery life and charge-discharge efficiency.

Secondly, battery materials, such as graphene materials which were popular in previous years, ternary lithium battery materials which are widely used now, and Ferrous lithium phosphate materials which are widely used by many manufacturers, especially those in China.

Third, it is the change of battery capacity caused by the temperature change of the battery. In the process of driving, we must ensure that the battery temperature is within the controllable range. At high temperature, the electrochemical reaction of the battery is accelerated, the electrolyte evaporates quickly, the electrode plate is easy to be damaged, and the overcharge phenomenon is easy to occur, which seriously affects the service life of the battery. Hot weather, coupled with the heat generated during charging, will lead to a very high temperature on the surface of the battery, scalding the protective shell on the surface of the battery, and even catching fire, so when charging, it must be charged in a cool and ventilated place. At low temperature, the viscosity of electrolyte decreases. When the conductivity decreases, the activity of the active substance will also decrease. It will increase the concentration difference of electrolyte, enhance polarization

and terminate charging ahead of schedule. More importantly, the diffusion rate of lithium ions at the carbon cathode will be slower. It is easy to precipitate lithium. When the temperature decreases, the reaction rate of the electrode also decreases. Assuming that the battery voltage remains constant and the discharge current decreases, the power output of the battery will also decrease.

The focus of this study is how to use the cooling system to stabilize the battery temperature in a range. That is the third point mentioned earlier. According to the standard of American Battery Association, the ideal temperature of battery in working state is 20-40 degrees Celsius.

1.1 Advantages of evaporative cooling system

Currently mechanical vapor compression (MVC) systems are dominant over air conditioning industry. As shown in fig.1. An intensive energy consumption and environmental issues are related to MVC. To overcome the energy consumption and environmental issues caused by emission of chlorofluorocarbons (CFC), it is necessary to find the efficient, low power consumption, and environmental friendly systems for air conditioning purposes. In this regard, evaporative cooling system has gained growing interest from last decades because it offers high energy efficiency and is environmental friendly benign. Various indirect evaporative cooling systems have found potential applications in air-conditioning systems, gas turbines,

electronic cooling, and cooling towers, and etc. Evaporative cooling is a novel technology that converts warm outside air into cool air by the latent heat of vaporization of water. Coefficient of system performance (COP) is much higher than that conventional mechanical compression cycle system.

The most commonly used evaporative coolers are direct evaporative cooler (DEC) and indirect evaporative coolers (IEC). In DEC, the product air comes in direct contact with water to facilitate latent heat of vaporization, hence the evaporation of water lowers the air temperature. This

system effectiveness is very high but accompanies with increased humidity to yield possible thermal discomfort for occupants. To ease the influence of humidity, indirect evaporative cooling system is used. Significant amount of efforts have been made in the past and recent studies tend to investigate and optimize IEC using vertical plates with sprayed water, IEC using horizontal plates with atomized water, IEC using horizontal tubes, R-IEC using horizontal plates, R-IEC using vertical plates, and other evaporative cooling systems. Besides, some innovative IEC systems comprising a thin aluminum foil have been developed that eliminate the need of hydrophilic surfaces.

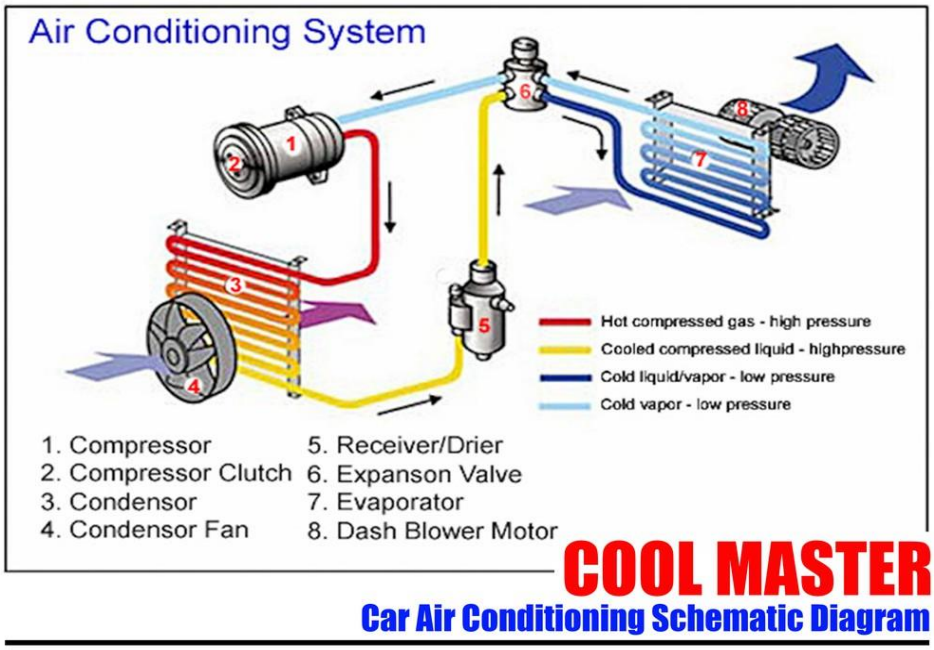

Fig.1. Schematic diagram of air conditioning system

1.2 Working principle of evaporative cooling system

Evaporative cooling can be divided into direct and indirect types.

Direct evaporative cooling (DEC) makes use of enthalpy of vaporization to raise the humidity (up to 70 to 90%) while reducing the dry bulb temperature. Typical DEC follows isenthalpic process alongside the psychrometric chart. To sustain the evaporation process, the humidified moist air should be constantly removed to the ambient. A mechanical direct evaporative cooler (M-DEC) as shown in Fig. 2 (a) accommodates appreciable wetted membranes or pads as the surface area which can enhance water evaporation rate considerably. Direct evaporative cooling is an open circuit process.

Indirect evaporative cooling is a closed circuit process. This employs the direct evaporative cooling plus a heat exchanger for the cooling purpose. The moist air from the direct evaporative cooling (DEC) makes a direct contact with the conditioned supplied air as depicted in Fig. 2 (b). The moist air is released to the ambient or cools by some external devices like solar cells. In this way, excess humidity is prohibited in enclosed spaces such as residential systems. Some of the potential applications of IECs including buildings are illustrated in Fig. 3. The potential applications include both human and non-human thermal comfort. Most of the studies included in the present review are related to the thermal comfort of human whereas very few studies regarding the applications of evaporative cooling in thermal management of livestock, poultry birds, and agricultural storage applications have been included in this study. The authors have assessed the potential of various evaporative cooling systems in applications like agricultural storage, poultry birds, and livestock.

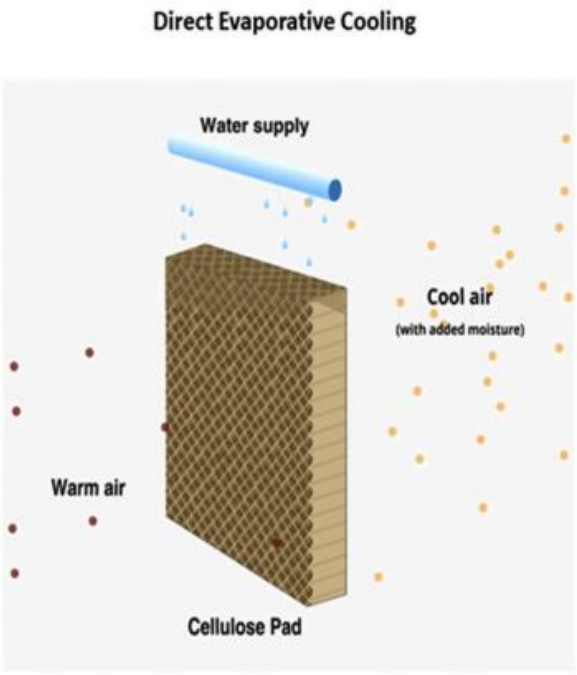

Fig.2 (a) DEC

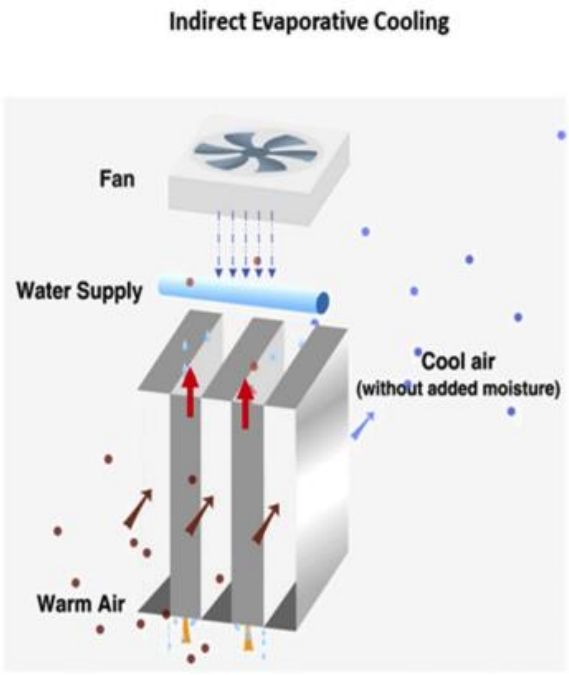

Fig.2 (b) IEC

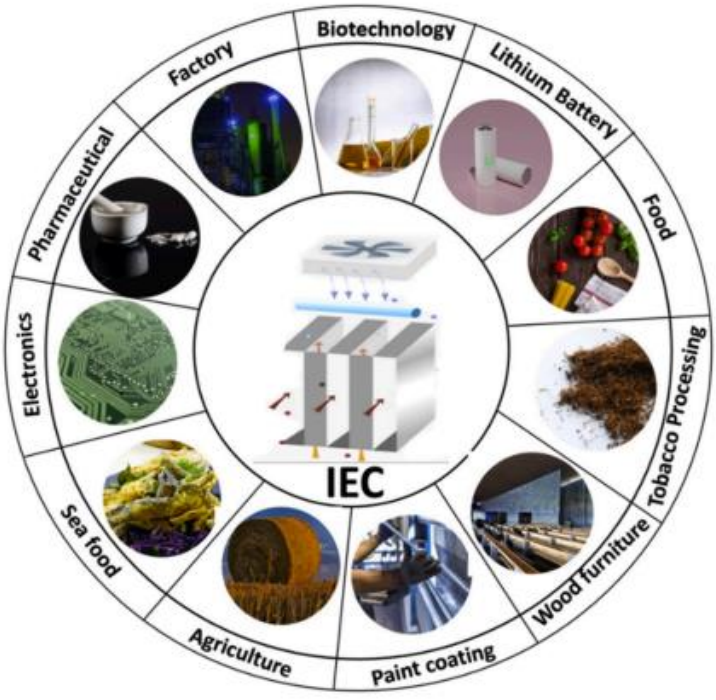

Fig.3 Applications of indirect evaporative cooling systems

Evaporative cooling technologies utilize the latent heat of evaporation to cool down the air without the need for compressor and cooling tower, realizing low electricity consumption while achieving the essential cooling power. For a typical evaporative cooling device, the COP in terms of electrical power can be as high as 15–20. Further more, no chemical refrigerant is used in evaporative cooling systems and they are deemed as environmentally friendly.

1.3 M-cycle

In this paper, we focus on the dew point evaporative cooling process that will eventually result in a potential technology for air cooling and yet without the use of any refrigerant-based compressor cycle.

As mentioned above, it can be divided into DEC and IEC.

However, DEC deals with air supply through isenthalpic humidification, which will lead to the increase of room humidity. IEC does not increase the moisture content of air supply, but the air supply temperature is higher and the wet bulb efficiency is lower. These shortcomings limit the application of DEC and IEC technology. The air supply of MIEC-M Cycle IEC can break through the wet bulb temperature of the inlet air and even approach its dew point temperature (therefore, it is also called dew point indirect evaporative cooling) without increasing the moisture content of the air supply.

The basic framework of M-cycle is shown in Figure 4.

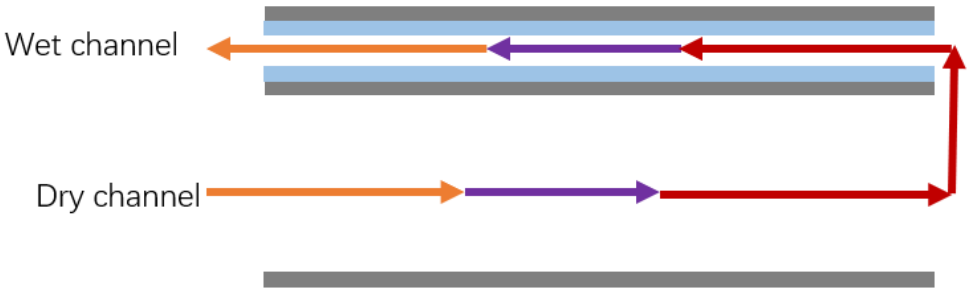

Fig.4. M-cycle evaporative cooling system

A single-stage dew point evaporative cooler for handling unsaturated air with counter-flow configuration（M-cycle）, as shown in comprises generically two air flowing channels and three air flowing streams, namely, (i) the supply air, (ii) the product air, and (iii) the working air. The supply air to be cooled is pushed through the dry channel where its temperature is lowered by water evaporation that occurs inside the adjacent wet channel. Part of this conditioned air is extracted as the product air whilst the remaining portion is employed as the working air to perform the evaporative cooling in the wet channel. Evaporation of water in the wet channel is primarily influenced by the partial pressure difference of water vapor between the air stream and the saturated air in the boundary layer of water film. The working air is almost saturated before leaving the channel. With such an arrangement, a sizable fraction of the initial supply air can be cooled to approach its dew point, a process differing from the conventional evaporative cooling.

The prototype of dew point evaporative coolers usually comprises several generic pairs of dry and wet channels with a stack arrangement. The separating plate between the dry and wet channels is made of hydrophobic materials, such as polyethylene or aluminum foil. On the wet-side, a thin wick material is overlaid to enhance wettability of the surface of wet channel. Because the M-cycle system is different from the traditional cooling system and does not use refrigerant, it is environmentally friendly and will not cause pollution. This is also in line with

the environmental protection concept of electric vehicles. At the same time, the cooling efficiency of M-cycle is far superior to the general IEC system, so in this study, we will use M-cycle to cool the target object.

1.4 On the selection reason of M-cycle counterflow device

Recently, dew point evaporative cooling has demonstrated better potential for an IEC with higher wet bulb effectiveness than 1.0.

Two viable flow configurations, i.e., cross flow and counter-flow arrangements, were adopted for dew point evaporative cooling process. Hsu et al. investigated three types of wet-surface heat exchangers, including unidirectional flow, counter-flow and closed-loop flow configurations. They reported that the maximum wet bulb effectiveness for counter-flow, cross-flow, and closed loop configurations is 1.3. Zhao et al. carried out a numerical study on a novel counter-flow heat and mass exchanger (HMX) with triangular air channels. They concluded that under a typical UK summer weather condition, the system could achieve the wetbulb effectiveness of up to 1.3. The effects of different parameters, such as air velocity, working-to-intake-air ratio and channel sizeon the cooling effectiveness were also studied. Duan studied the dew point indirect evaporative cooler for building applications.

The cooler was simulated and tested under different controlled parameters. It was found that the wet bulb and dew point effectiveness varied from 0.55 to 1.10 and 0.40 to 0.85, respectively, with COP ranging from 3 to 12. Riangvilaikul and Kumar performed numerical and experimental studies on dew point evaporative cooling using different inlet air temperature, humidity and velocity, and the wet bulb effectiveness was found to be in the range of 0.92–1.14. Their proposed design performed well under dynamic conditions. Lee and Lee proposed a counter-flow regenerative evaporative cooler with finned channels, and their experiment showed that under the inlet condition of 32 C and 50% RH, the

outlet temperature was 22 C, below the inlet wet bulb temperature of 23.7 C. Zhan et al. compared the counter-flow and cross-flow dew-point cooling configurations, and evaluated their effectiveness, COP, and cooling capacity. From their simulation results, the counter-flow configuration provides better effectiveness and larger cooling capacity without significant increase in energy consumption, compared to cross-flow system. Jradi and Riffat presented a two-dimensional numerical model for a cross-flow dew point evaporative cooler, and results were validated by the experimental data from the cooler. They stated that the wet bulb effectiveness of the cooler was 1.12 with 2017 W of cooling capacity under the inlet air condition of 30 C and 50% RH. Hasan proposed an analytical model using modified e-NTU method, as well as the numerical method, to study the counter-flow dew point evaporative cooler. It was found that the results from the two models were similar, and agreed well with the experimental data.

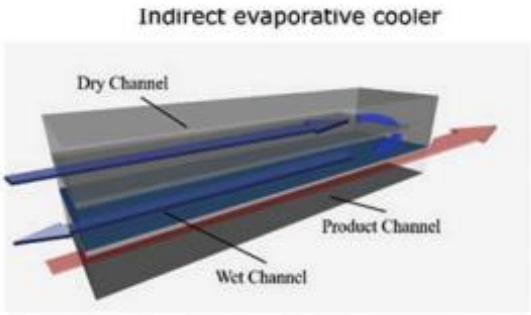

M-cycle counterflow arrangement

1.5 Ternary lithium battery

Before choosing a suitable battery object, it is necessary for us to know the type of battery first, so as to make a better choice. The current batteries can be divided into two camps according to their packaging shapes, different cathode materials and different internal electrode stacks, namely ternary lithium batteries and lithium iron phosphate batteries. Now let's

understand their structures and characteristics one by one.

Tesla is currently widely using ternary lithium batteries. Because this battery has high density, light weight and good endurance. Its biggest disadvantage is that its safety and stability are slightly poor, and it is unconventional. More importantly, it is prone to fire and explosion.

Fig. 5 shows ternary lithium batteries 1865, 2170 and 4680 for Tesla vehicles.

Fig.5. Ternary lithium battery

In contrast, it is a lithium iron phosphate battery. At present, this kind of battery is mainly popular among electric vehicle manufacturers in China.

The reason why new energy vehicles will be equipped with lithium iron phosphate batteries at first is that the cost of such batteries is not high, and the service life and safety are good, and the current lithium iron phosphate batteries also maintain these advantages. The disadvantage is that the free amount of lithium ions in the electrolyte of the cathode material of lithium iron phosphate battery will be affected by low temperature. Simply put, if the temperature is too low, the capacity of lithium iron phosphate battery will decrease, and the capacity at 0℃ is only about 65% of the normal one, and the capacity at -10℃ is only about 50%, which is still quite significant.

As shown in Figure 6, it is a general lithium iron phosphate battery.

Fig.6. lithium iron phosphate battery

1.6 Blade battery

"Blade battery" is actually a lithium iron phosphate battery, so it is named because of its long external length and thin thickness. Compared with the traditional battery pack, the volume utilization rate of "blade battery" has increased by more than 50%, that is to say, the cruising range can be increased by more than 50%, reaching the same level of high energy density ternary lithium battery. While improving the energy density of the battery, it keeps the properties of lithium iron phosphate battery such as high temperature resistance and non-flammability, and has higher safety than ternary lithium battery. The volume energy density is 50% higher than that of the traditional lithium iron battery-equivalent to a car that can run 400 kilometers, and now it can run 600 kilometers.

In the field of battery testing, the most difficult needle test requires a steel needle to pierce the battery core, resulting in a large area of short circuit inside the battery core. In the test video, the temperature of ternary lithium battery changed dramatically at the moment of acupuncture, and the surface temperature quickly exceeded 500℃, and the eggs placed on the battery surface were blown up. After the traditional block lithium iron phosphate battery was punctured, there was no open flame, but smoke came out. At the same time, the surface temperature of the battery reached 200-400℃, and the eggs on the battery surface were scorched at high temperature. However, after the blade battery was punctured, the surface

temperature remained at a stable level of 30-60℃, and there was no smoke or fire, and the eggs on the battery surface were still in a flowing state.

On the stability of the lithium iron battery itself, the blade battery is made into a thin strip with a larger heat dissipation area. At the same time, the battery loop is long and the heat is not easy to concentrate on the circuit, so it can maintain a stable temperature after being punctured, and the safety performance is greatly improved.

The size of the blade battery are shown in Figure 7 below.

Figure.7. Blade battery size

Related parameters of blade battery are shown in Figure 8 below.

Modle: 3.2V138Ah LiFePO4	Discharge Cut-Off Voltage: 2.0V
Standard Voltage: 3.2V	Continuous Discharge: 138A
Rated Capacity: 138Ah	Internal Resistance: ≤1.8mΩ
Weight: 2.63±0.1kg	Charging Temperature: -10~50℃
Charging Voltage: 3.65V	Discharge Temperature: -20~55℃

Figure.8. parameters of blade battery

To sum up, we can draw the following conclusions.

1. Compared with the ternary lithium battery with incomplete technical development at present, the blade battery has better power performance.
2. The blade battery has certain security. (Accidents such as burning and explosion are not easy to occur.)
3. In the study, the regular shape of blade battery is more conducive to analyzing its heat transfer direction.

Therefore, this study will select the blade battery as the research object. The blade battery is put into the evaporative cooling M-cycle to study whether the M-cycle has the ability to cool the working battery and keep it at a certain temperature so that it will not fail.
At the same time, explore when the cycle can reach a steady state. Including the time to reach steady state and the temperature change of dry and wet channels.

1.7 Soft-pack batteries

The soft-pack battery is a name compared with the cylindrical and square hard-shell batteries. Its internal composition (positive electrode, negative electrode, separator and electrolyte) is not much different from that of the square and cylindrical lithium batteries. The biggest difference is that the soft-pack battery uses aluminum-plastic composite film as the shell, while the square

and cylindrical batteries use metal materials as the shell. What are the advantages and disadvantages of flexible battery? Funeng Technology summarized four advantages and three disadvantages of flexible battery in the prospectus. Advantages mainly focus on high energy density, good safety, small internal resistance and flexible design. First of all, the energy density is high. GGII data shows that the average energy density of ternary soft-packed dynamic battery produced in the power battery industry has reached 240-250Wh/kg, but the energy density of ternary square power battery with the same material system is 210-230Wh/kg. The energy density of single cell of ternary flexible battery is 10%-15% higher than that of ternary square battery. Secondly, the safety performance is good. Under the same material system, when the ternary soft-package power battery is packaged with aluminum-plastic film soft-package, if the battery thermal runaway occurs, it generally flattens to release heat; However, because the square and cylindrical batteries are packed in hard shells, the heat cannot be released, and the internal pressure is high, which will cause explosion. In addition, with the increase of battery service time, the square and cylindrical batteries with winding production process are more likely to have different internal temperatures and uneven stress distribution, especially at winding bends, thus creating potential safety hazards. Thirdly, the ternary flexible battery has the advantages of large capacity and small internal resistance. Because of the small internal resistance, ternary soft package power battery can greatly reduce the self-consumption of the battery, improve the battery rate performance and cycle life, and generate less heat. Fourthly, on the battery cell level, the size and shape design of the battery cell of ternary soft package power battery are flexible. Enterprises can customize according to their own product design and customer needs. At the level of module and battery pack, the space layout of ternary soft package power battery is more flexible, which can be rectangular or T-shaped, and can meet the space requirements of more vehicles for power batteries. Disadvantages are reflected in three aspects: more complicated technology, low group

efficiency and high cost. For example, the packaging link is difficult to control, and it is easy to swell, which makes the product consistency poor and puts forward higher requirements for the technical level and manufacturing process of the enterprise; Compared with the square and cylindrical power batteries with the same material system, the grouping efficiency of ternary flexible battery is relatively low; The battery core of ternary soft package power battery has poor self-protection, and it is easy to be punctured in extreme cases. Therefore, it is necessary to add metal protective layer to the battery package to give more protection, which will bring about the problem of rising cost.

Soft package power battery

In view of the shortcomings of flexible battery, this study will not involve flexible battery.

Chapter 2: Construction of Cooling System Based on M-cycle

In this chapter, the arrangement of batteries, the concrete structure of M-cycle cooling cycle and the related heat transfer relationship will be elaborated in detail. At the same time, a new system hypothesis of M-cycle evaporative cooling cycle will be given for power battery cooling.

Part of the structure of the original M-cycle is optimized.

2.1 The new M-cycle system

In the previous article, we explained the working principle of M-cycle and related cycles in detail. In this section, a new M-cycle structure will be proposed according to M-cycle cycle theory.

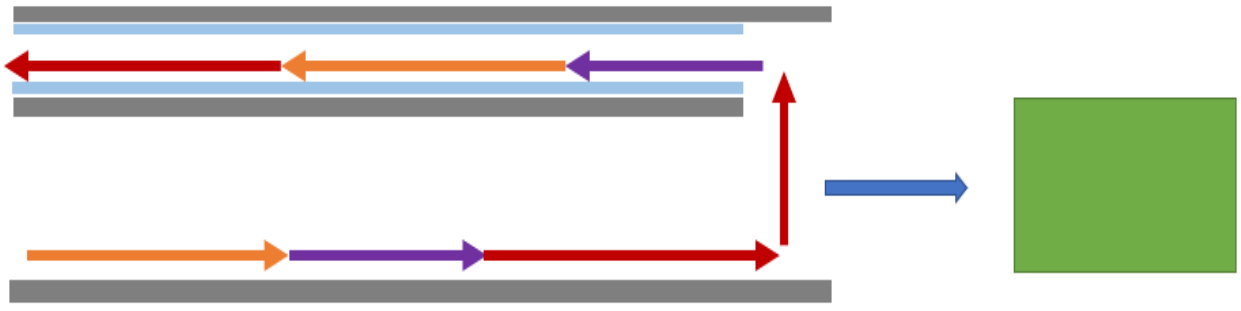

Figure.9. Traditional M-cycle cycle

First, as shown in Figure 9, it is a traditional M-cycle cycle. In this cycle, the air enters from the lower left along the orange arrow, and when it enters the end of the dry channel, 30% of the

air will enter the wet channel for evaporation and heat exchange. The remaining 70% air will flow into the next unit. It should be noted here that the next unit refers to the object that needs to be cooled by the M-cycle system.

Regarding this study, the cooling object is BYD's blade battery. However, it is different from the traditional situation that the cooled object is outside the system. In this M-cycle, we will put the blade battery into the dry channel for cooling. Because the target object is inside the cooling cycle, the semi-open cycle shown in the traditional M-cycle will be meaningless. Therefore, the system used in this M-cycle will be changed into the form of closed cycle. In other words, all the air entering the dry channel will enter the wet channel for circulation. Fig. 10 is a diagram of a new M-cycle system dedicated to battery cooling.

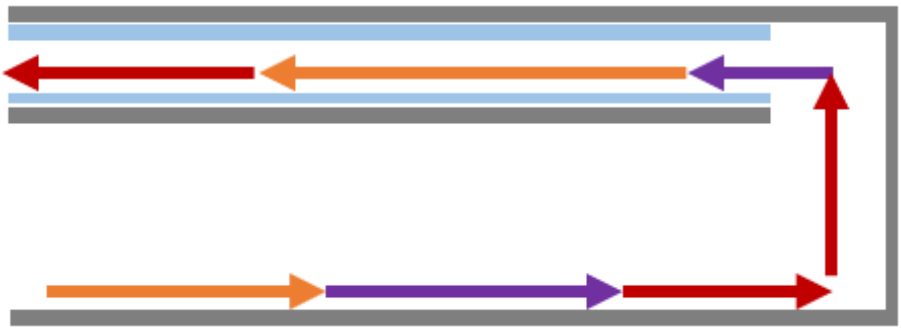

Figure.10. M-cycle cooling box

This new MIEC cycle can be called M-cycle cooling box. As shown in the figure, after the air enters the dry channel, there is no working air output in the process of flowing to the wet channel, and all the air will be used for cooling cycle.

2.2 Arrangement of batteries

After determining the system structure, we need to determine the arrangement of cooling objects, that is, batteries, in the system. As mentioned earlier, due to the regularity of BYD

blade battery shape, it is beneficial to calculation and simulation. BYD blade batteries are rectangular, so there are only three arrangements. That is, according to the length, width and height of the battery. As shown in figure 11.

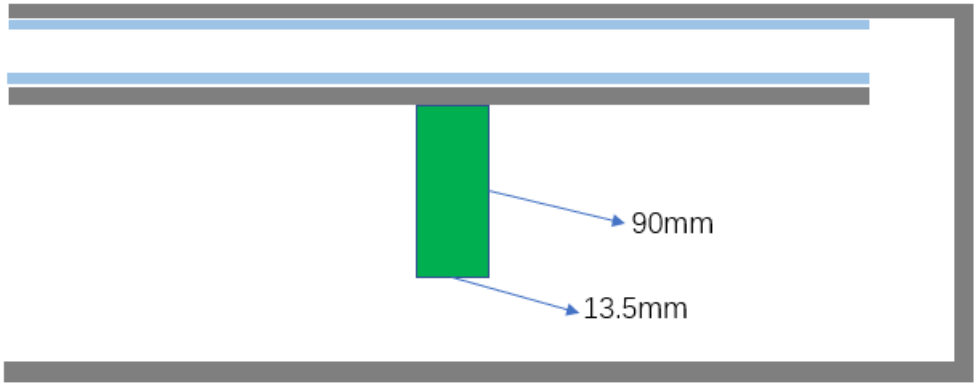

figure 11. Battery arrangement form(1)

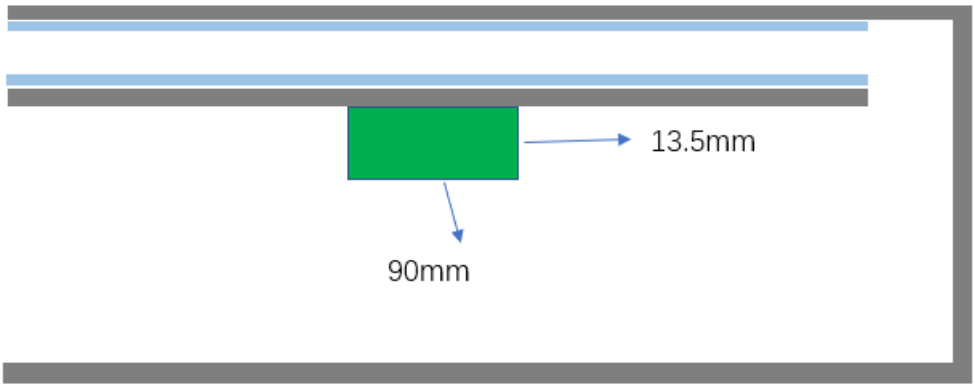

figure 11. Battery arrangement form(2)

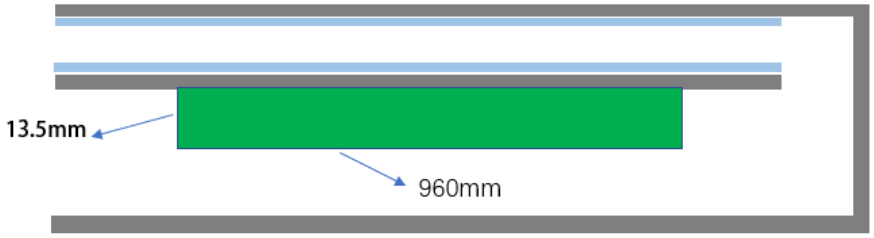

figure 11. Battery arrangement form(3)

The common point of the three arrangements is that one side of the battery is close to the wall. According to its size, the layout method is slightly different. According to the heat transfer formula (1), the larger the heat dissipation area, the better the heat dissipation effect.

$$\emptyset = hA\Delta T \quad (1)$$

In formula (1), A a is the heat transfer surface area, h is the thermal convection coefficient, and T is the temperature change. That is, high temperature and low temperature. $\emptyset$ is heat. Therefore, it is obvious that the arrangement of Figure 11(3) is more in line with the formula. To sum up, the final arrangement is that the battery body with a length of 960mm and a thickness of 13.5mm is attached to the wall, and the contact area between the wall and the battery is 960mm multiply by 90 mm.

The final arrangement is as shown in the figure .12.

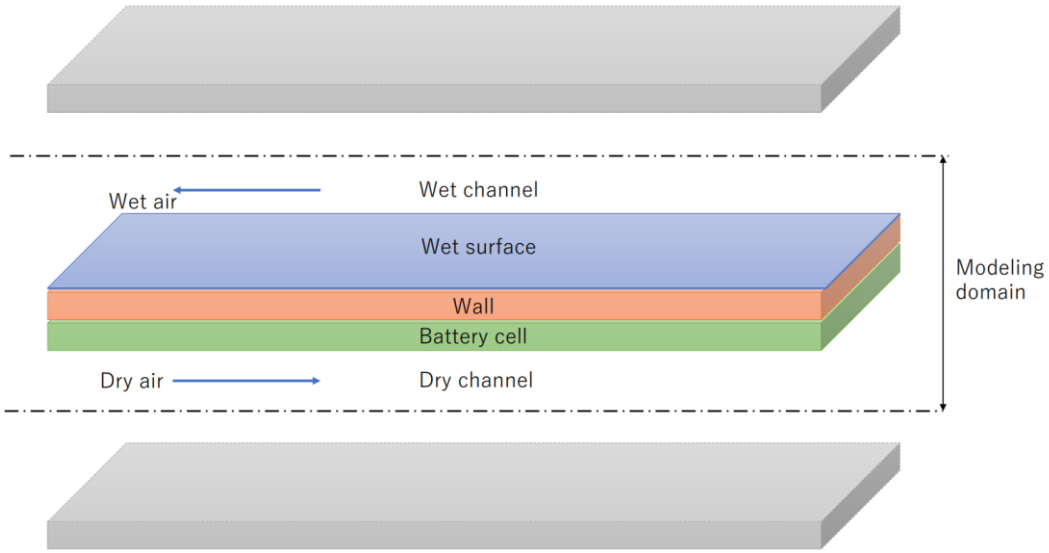

figure 12. Final arrangement mode

2.3 Some supplementary data of M-cycle cooling box.

Fig. 12 shows the research structure of M-cycle.

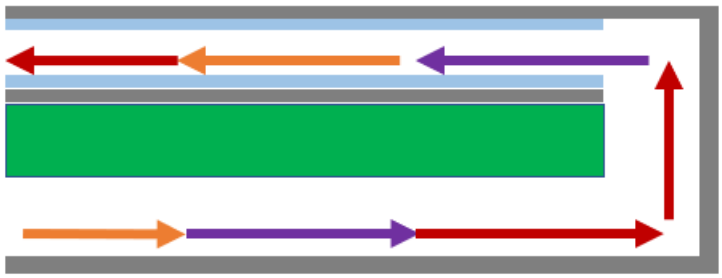

figure 13. structure of M-cycle

As shown in Figure 13, the original model is simplified and improved, and the final structure is obtained. The change point will be explained below.

The first is the height of dry and wet channels. According to predecessors' experience, the air circulation height of dry channel is 5mm, and that of wet channel is 2.5 mm.

Then, in order to calculate the air volume in the channel, the length of the dry and wet channel is equal to the length of the battery, that is, 960 mm. The length of dry and wet channels is also

equal.

Finally, for the convenience of calculation and simulation. The part of the blue water film can be regarded as approximately non-consumption.

Chapter 3: Mathematical model of M-cycle cooling box

In this chapter, the heat generation and heat dissipation of the battery in the M-cycle cooling box will be analyzed one by one. The detailed calculation formula and method are given. Because M-cycle cooling box is different from traditional M-cycle countercurrent cooling, the calculation method of heat source will be extremely important.

3.1 The heat transferred to the air by the battery in the dry channel.

As the most important part, we will first explore the calculation method of battery heating.

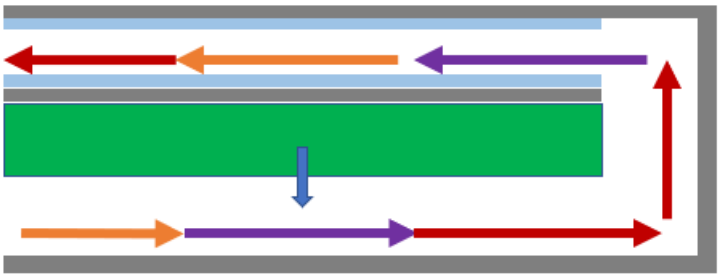

figure 14. The battery transfers heat to the dry channel air.

The battery transfers a part of heat in the dry channel downward along the Y-axis direction, that is, in the air. As shown by the blue arrow in fig. 14

Let's calculate the heat in the dry channel first.

Let the battery temperature be Tb. Tb0 is the initial temperature of the battery before operation, which can be approximately equal to room temperature.

According to the basic formula of thermodynamic formula(1)

$$Q = CM\Delta T \quad (1)$$

It is known that if you want to know the temperature of the battery in the dry channel, then it can be seen that if you want to know the temperature of the battery in the dry channel, you can transform the formula into formula(2)

$$T = \frac{Q}{CM} \quad (2)$$

Where Q is the total heat, C is the specific heat capacity of the battery, and M is the battery mass. Because the battery itself has an initial temperature before working, the initial temperature of the battery and the part that generates heat during working are calculated separately.

Therefore, assuming that the temperature of the battery itself is Tb0, the following formula (Formula 3) can be obtained.

$$Tb = T_{bO} + \frac{\emptyset \times t - hA \times \Delta T}{m \times C_b} \quad (3)$$

Tb0 represents the calorific value of the battery per unit time.

t stands for battery working time.

h is convective thermal conductivity.

A is the heat transfer surface area.

△T is the temperature difference, that is, the difference between the room temperature and the actual working temperature of the battery.

Cb is the specific heat capacity of the battery.

In Formula 4, the fractional part represents the heat energy transferred by the battery to the air

during operation.

Here △T represents the temperature difference, which can be written as Formula 4.

$$\Delta T = T_b - T_{din} \quad (4)$$

Tdin in formula (4) represents the air inlet temperature, that is, the room temperature.

Regarding Cb, since the shell of the blade battery is made of aluminum, it can be considered that the specific heat capacity of the blade battery is that of aluminum.

$$h = \frac{\lambda}{l} \times Nu \quad (5)$$

$$Nu = 0.664 Re^{1/2} Pr^{1/3} \quad (6)$$

$$Re = \frac{V \times l}{\nu} \quad (7)$$

Formulas (5), (6) and (7) are used to calculate Nusselt number, Reynolds number and thermal convection coefficient respectively.

Among them, the coefficient of 0.667 in Formula (6) is selected mainly because the air flow in the dry channel conforms to the laminar flow condition in this study.

In the formula (5), λ is the thermal conductivity of the battery.

In formula (6), Pr is Prandtl Number.

In formula (7), V is the air flow rate and l is the battery length, that is, 960 mm. Denominator V is aerodynamic viscosity.

It's over here. We have calculated the heat of the part of the battery radiating to the air in the dry channel.

3.2 Heat transfer in wet channel

As shown in fig. 15, the battery clings to the upper wall of the dry channel, and a part of the heat is transferred to the wet channel through the wall, which causes the temperature to rise and causes the water to evaporate. Therefore, the energy required to evaporate water in the wet channel is the total energy of heat transfer from the battery to the wet channel. The yellow arrow indicates the heat transfer direction.

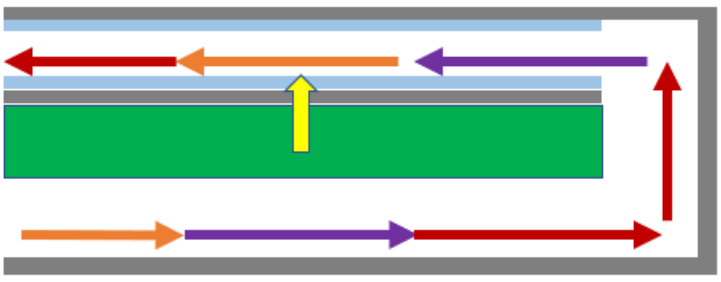

figure 15. The battery transfers heat to the wet channel through the wall.

Firstly, the volume of air in wet channel is calculated.

Let the density of air be ρ, the height of wet channel be Hw and the width be D. The width here is the width of the battery, 90 mm.

l is the wet channel length, that is, the battery length, that is, 960 mm.

Finally, the following formula can be obtained.

The air mass in the wet channel

$$H_w \times D \times l \times \rho \quad (8)$$

Let h" be the enthalpy of steam and h is the enthalpy of water, and their difference is the heat absorption of water when it becomes steam.

Enthalpy required for vaporization of liquid water can be written as formula (9)

$$(h''\text{-}h) \qquad (9)$$

Finally, let the humidity at the outlet of the wet channel be d', d is the humidity of the inlet air of the wet channel.

The humidity difference is

$$(d'\text{-}d) \quad (10)$$

To sum up, multiply all the above formulas to get the heat that needs to be absorbed by the actual evaporation of water in the wet channel, that is, the heat transferred from the battery to the wet channel. Such as formula (11)

$$H_w \times D \times l \times \rho \times (h''\text{-}h) \times (d'\text{-}d) \quad (11)$$

Formula (11) is all the heat transferred from the battery to the wet channel.

Wet channel inlet temperature is equal to dry channel outlet temperature.

Let the outlet temperature of dry channel be Tdout and the inlet temperature of wet channel be Tdwin

The relation can be written as

$$T_d out = T_d w_i n \quad (12)$$

$$T_d out = \frac{hA\Delta T}{Ca} \quad (13)$$

In formula (13), Ca is the specific heat capacity of air.

The enthalpies of liquid water and water vapor, as well as the air pressure can be obtained by looking up the table from the temperature.（Refer to appendix）

Chapter 4: Simulation result analysis

In this chapter, through the formula analysis in Chapter 3, we have got a general understanding of the heat generation and transfer relationship of the whole system. In this chapter, the previous conclusions will be used for data analysis. The analysis tool is MATLAB.

In fact, M-cycle cooling circulation box is a system with two cycles. That is, the superposition of traditional air-cooled cycle and M-cycle. When the system works, two air-cooled systems will work at the same time.

4.1 On the simulation results of the cycle.（Air cooling cycle）

First of all, we only simulate the air cooling of the main channel.

Because it is a pure air-cooled cycle, the wet channel is not considered for the time being.

After programming the above formula, the following results can be obtained (as shown in Figure 16).

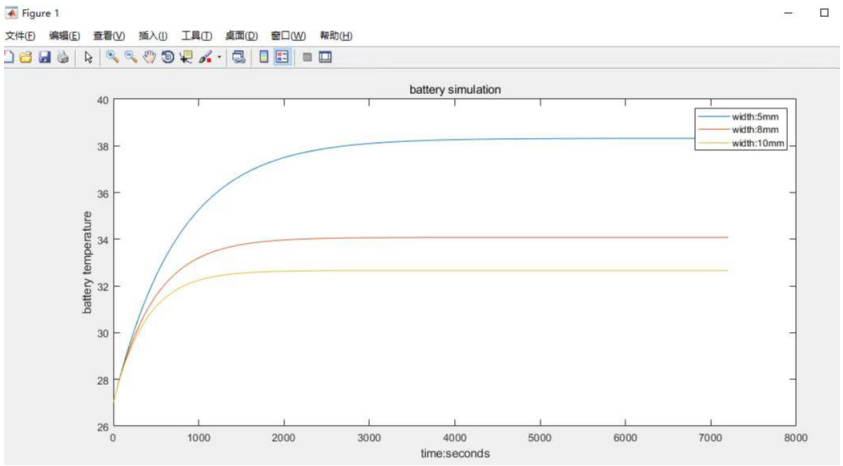

figure 16. Battery temperature simulation curve(air cooling system)

```
channel_len = 0.96;   % len of channel, meter
channel_width = 0.09; % width of channel, meter
channel_height_dry = 0.005;  % meter
channel_height_wet = 0.0025; % meter
m = 2.63;            % kg, weight of battery
cp = 880;            % Specific heat capacity of battery
v_air = 3;           % m/s
temp_room = 27;      % centigrade
h_water = 4.17;      % KJ/kg
h_vapour= 2550;      % KJ/kg
lambda =  237;       % w/mk, Thermal conductivity of battery
I = 138;             % current
R = 1.8e-3;          % battery resistence
```

figure 17. Important parameters used in simulation

As shown in Figure 17, it is an important parameter used in the simulation, in which the channel length and width are consistent with the battery parameters, that is, the length is 960mm and the width is 90 mm. The height of dry channel is 5mm, the height of wet channel is 2.5mm, and the total mass of battery is 2.63KG. The specific heat capacity of the battery is 880, which is obtained from the look-up table. Because the surface of the whole battery is wrapped by aluminum, the specific heat capacity of aluminum is adopted. The air inlet velocity is tentatively set at 3m/s. The room temperature is 27℃, the continuous discharge current is 138A, and the internal resistance is 1.8mΩ.

The above are the shape parameters and initial conditions.

According to the initial conditions in fig. 17, the graph shown in fig. 16 can be obtained after MATLAB simulation.

The blue part of the figure shows the temperature change curve of the battery when the air circulation height of the main channel is 5 mm.

Let's first observe the blue curve, which is the curve when the main channel is 5 mm. As can be seen from the figure, the temperature of the battery finally stabilized at around 39 degrees Celsius. When the system starts working until it reaches a stable state, it takes about 50 minutes. It can be clearly seen from the figure that after 50 minutes, the curve tends not to change dramatically. At this time, the battery temperature meets the requirements of the American Battery Association below 40 degrees Celsius, and also meets the requirements of the American automobile website Freedom car that it should not be higher than 52 degrees Celsius. Therefore, according to the simulation results, it is theoretically possible for the new M-cycle cooling box to cool the single power battery in the working state.

4.2 Influence of changing the channel height on the system. (air cooling system)

Through the control variable method, we can change a certain value under the condition of keeping the other values unchanged, and observe how much influence the change of this value will have on the whole system. In this study, we will also use this method for research. First, we adjust the height of the main channel from 5mm to 8mm and 10 mm. To explore the influence of the height change of the main channel on the system.

The red and yellow curves in Figure 15 correspond to the heights of the main channel of 8mm and 10mm respectively. It can be seen from the figure that the battery temperature finally stabilized at about 33 degrees Celsius when the height of the dry channel was changed to 8 mm.. The time for the system to reach steady state is 25 minutes. The yellow curve shows that the height of the dry channel is 10mm, and it can be obtained that the temperature of the battery finally stabilizes at about 32 degrees. The time for the system to reach steady state is 16 minutes. Comparing the three battery temperature curves with the height of 5mm, 8mm and 10mm, we can draw a rule that expanding the height of the dry channel will make the system enter the steady state faster. At the same time, the refrigeration effect is better. At the same

time, from the cooling temperature of the battery, compared with the curve of 5mm, the curve of 8mm has greatly improved the time for the system to reach the steady state and the cooling effect of the system on the battery. However, from 8mm to 10mm, its refrigeration effect is not obvious. It can be concluded that the refrigeration effect and the time required to reach the steady state will be greatly improved when the system is about 8mm in the main channel. If we continue to expand the height of the main channel, the income will decrease.

4.3 Influence of wind speed change on system refrigeration (air cooling system)

In practical application, because the application scene of power battery is electric vehicle. However, when the electric vehicle is actually running, the wind speed will inevitably increase, which will lead to the faster air flow in the cooling box. Therefore, this time we will control the change of wind speed to explore the impact on the cooling effect.

As shown in fig. 18

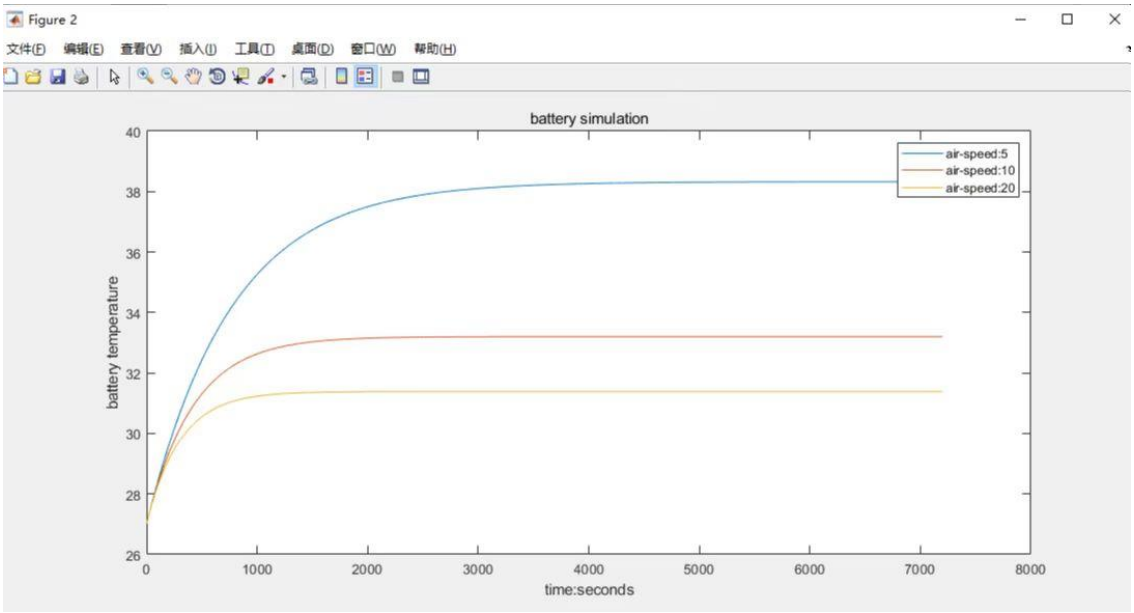

figure 18. Influence of wind speed change on system refrigeration (air cooling system)

The blue curve represents the wind speed of 5m/s, the red curve represents the wind speed of 10m/s, and the yellow curve represents the wind speed of 20m/s.

Let's analyze the blue curve first. As shown in Figure 17, when the wind speed is 5m/s, it takes 50 minutes for the system to reach the steady state, and the battery temperature is 38 degrees Celsius. When the wind speed is increased to 10m/s, it takes 25 minutes for the system to reach the steady state, and the battery temperature is 33 degrees Celsius. When the wind speed is increased to 20m/s, it takes 16.67 minutes for the system to reach the steady state, and the battery temperature is 31 degrees Celsius. According to the data in Figure 17, similar to the case of changing the height of the main channel, when the wind speed is higher, the time taken for the system to reach the steady state will be shorter and the final working temperature of the battery will be lower. But there is also a peak return. From the results, when the wind speed is increased to 10m/s, the time taken for the system to reach the steady state is obviously shortened, and the battery temperature is also lower. However, when the wind speed continues to increase, the time consumption is obviously reduced, and the battery temperature is only reduced by 2 degrees Celsius. It can be seen that increasing the wind speed in the system will really affect the refrigeration efficiency of the system.

4.4 Influence of changing battery discharge current on system refrigeration (air cooling system)

At present, there are many different situations about the continuous output current of blade battery. This time, the battery continuous discharge current calibrated in Figure 8 is selected. That's 138 amps. At the same time, according to the online inquiry, the normal working current of the blade battery is 27 amps. Therefore, this control variable method will change the discharge current of the battery to explore the influence on the refrigeration results of the system.

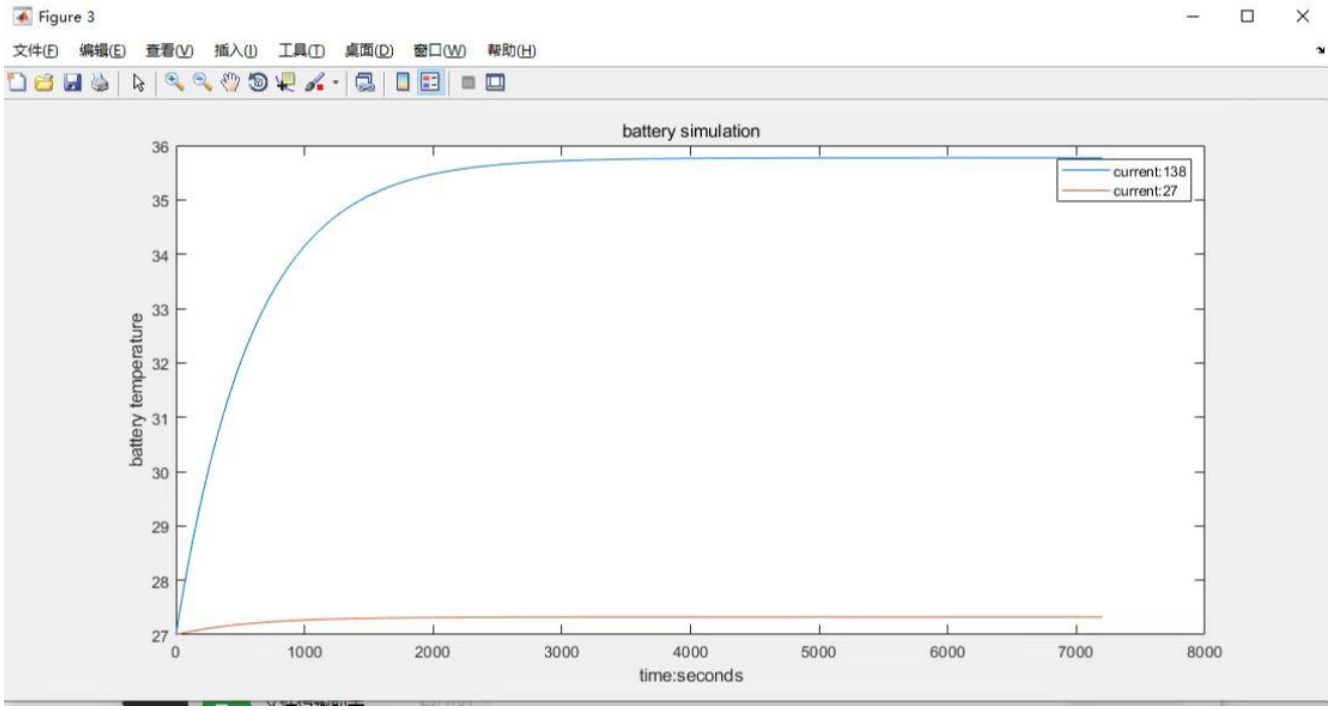

figure 19. Influence of current on system cooling(air cooling system)

As shown in fig. 19, it is the temperature change curve of the battery when the continuous discharge current is 138 amps and 27 amps. The blue curve is 138 amps and the red curve is 27 amps. It can be seen from the figure that when the discharge current is 27 amps, its surface temperature is close to room temperature, which is 27 degrees Celsius given by the initial conditions. It takes 16.67 minutes to reach steady state. When the working current is increased to the continuous discharge current of 138 amperes as shown in Figure 8, the battery temperature finally reaches 36 degrees Celsius. It takes 50 minutes to reach steady state. According to the data in fig. 18, when the discharge current increases, because the battery itself has internal resistance, increasing the current will increase the power consumption, resulting in serious battery heating. Therefore, during driving, avoiding stepping on the accelerator to accelerate can effectively control the heating degree of the battery.

4.5 Simulation result analysis (M-cycle)

Now we add the wet channel of M-cycle to study the change of battery temperature when two air-cooled systems work at the same time.

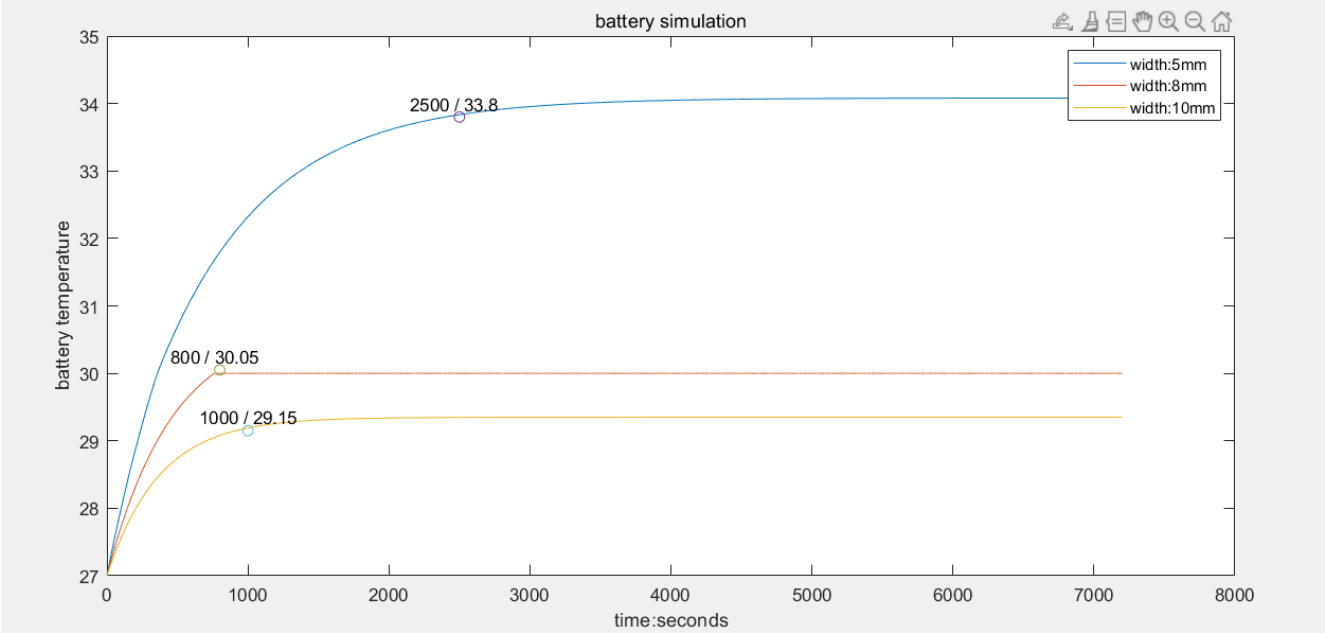

figure 20. Influence of changing the size of dry channel in M-cycle cooling box on cooling

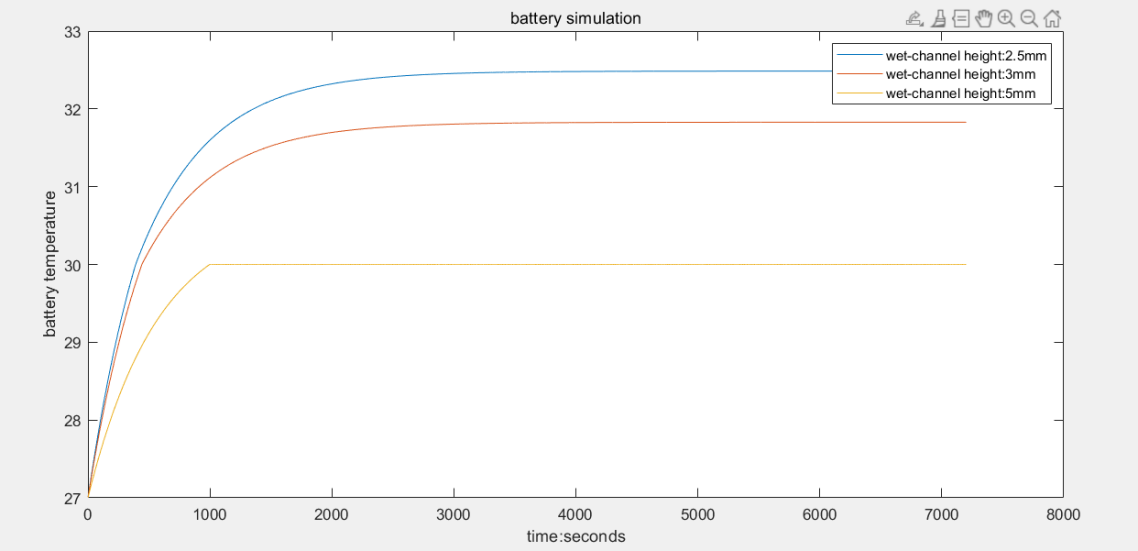

figure 21. Influence of changing the size of wet channel in M-cycle cooling box on cooling

As can be seen from figs. 20 and 21, the temperature of the battery is significantly reduced

after considering the influence of the wet channel. The simulation results show that the M-cycle cooling box has good cooling capacity.

As before, we change the wind speed and battery discharge current in the cycle to observe the influence on the cooling cycle.

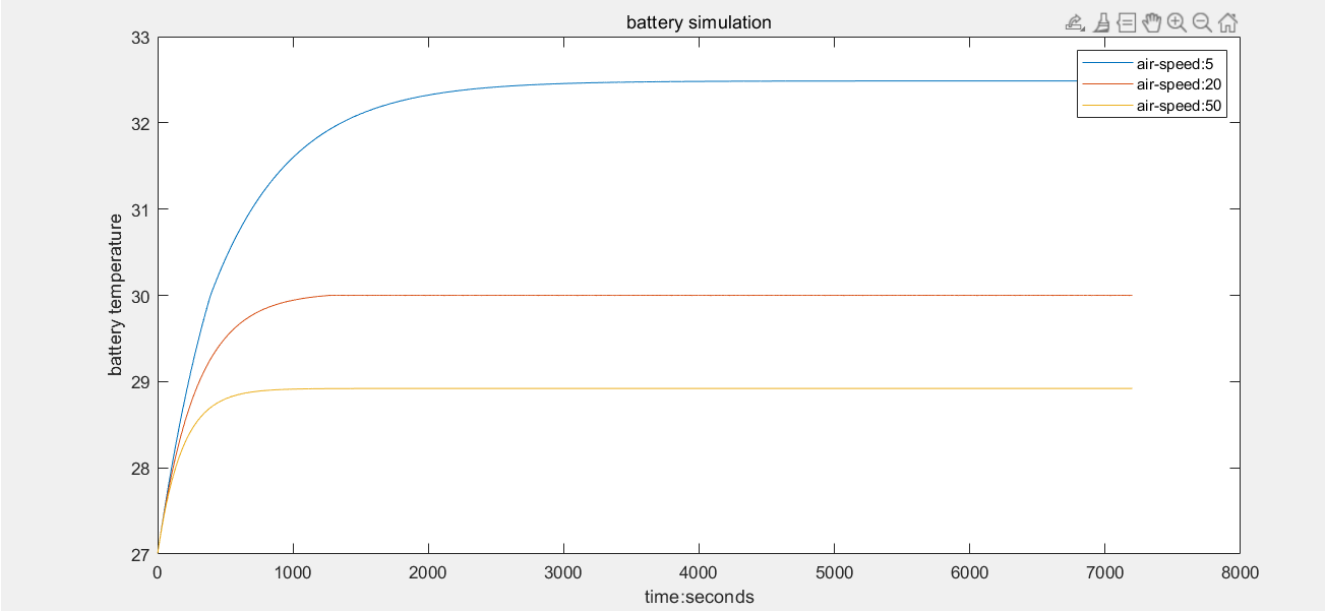

figure 22. Influence of changing wind speed on M-cycle cooling box

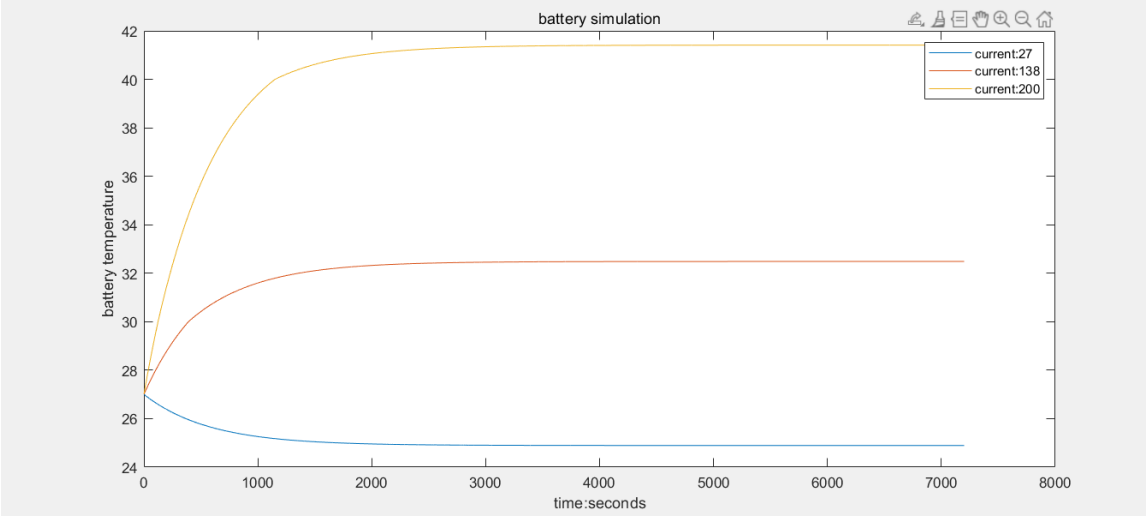

figure 23. Influence of changing current on cooling of M-cycle cooling box

From Figures 23 and 24, it can be concluded that increasing the wind speed is still effective for improving the refrigeration efficiency of the M-cycle cooling box. The increase of current will still increase the battery temperature. However, it is undeniable that the M-cycle cooling box with double circulation has stronger cooling ability for cooling objects. The shorter the time required for the system to reach the steady state.

Chapter 5： conclusion

In this chapter, the above simulation results will be summarized, and some possible conjectures will be given based on some simulation results and practical application.

According to the above description, we understand the specific thermal relationship of the new closed M-cycle cooling box. According to the given calculation formula, the final surface temperature of the battery is equal to the initial temperature of the battery minus the heat transferred to the air in the dry channel, that is, the thermal convection between the battery and the air. After subtracting the heat transferred by the battery along the Y axis, that is, the heat transferred by the battery to the wet channel through the inner wall (heat conduction. The heat transferred upward along the wall is finally estimated by the mass of evaporated water.

Through the cooling characteristics of M-cycle and the related simulation data, we can draw the following conclusions.

1. Because the cooling efficiency of M-cycle is directly related to the humidity of the inlet air, the lower the relative humidity of the inlet air, the better the ability of air to carry water vapor in the wet channel. So that that cool efficiency of the system is higher.
2. The system simulation shows that the cooling efficiency of the system can be improved when the height of dry and wet channel is changed.

3. Considering that the application scenario is vehicles such as electric vehicles, it can be predicted that the wind speed at the air inlet will become faster due to the increase of

driving speed. The simulation shows that when the wind speed is increased, the cooling efficiency of the whole system will also be improved, but the improvement is not linear, but there is a profit inflection point. When the wind speed exceeds the inflection point, the cooling efficiency improvement is not obvious.

4. Changing the working current of the battery can also affect the final cooling effect of the system. According to the simulation diagram, when the discharge current of the battery is 27 amps, the battery temperature is close to room temperature. When the discharge current is 138 amps, the battery temperature rises obviously.

5. By simulating the pure air cooling cycle and the double cycle of M-cycle cooling box, it can be predicted that the cooling capacity of M-cycle cooling box is far stronger than that of pure air cooling cycle.

Chapter 6： For the shortcomings of this study and the possible direction of future research

In this chapter, the shortcomings of this study will be summarized. At the same time, the possible extension direction of this study in the future is prospected for researchers' reference.

6.1 The shortcomings of this study

1. During this study, due to the limited time, the income inflection point of the expansion value of the main channel was not studied, and only the approximate range, that is, between 8 mm and 10 mm, was given.
2. Similarly, in this study, the inflection point of the increased wind speed income has not been fully proved, and only the approximate range can be given, that is, between 10 and 20 m/s.

The above are the shortcomings of this study.

6.2 possibility for in-depth optimization of closed M-cycle cooling system.

In view of the characteristics that M-cycle needs dry air, in areas with high humidity, such as Shanghai or Fukuoka, a dehumidifier can be added at the air inlet, which contains dehumidifying materials for air pretreatment. This change can greatly increase the cooling capacity of the whole cycle, and at the same time greatly improve the applicability of M-cycle for use in high humidity areas.

As shown in fig. 24

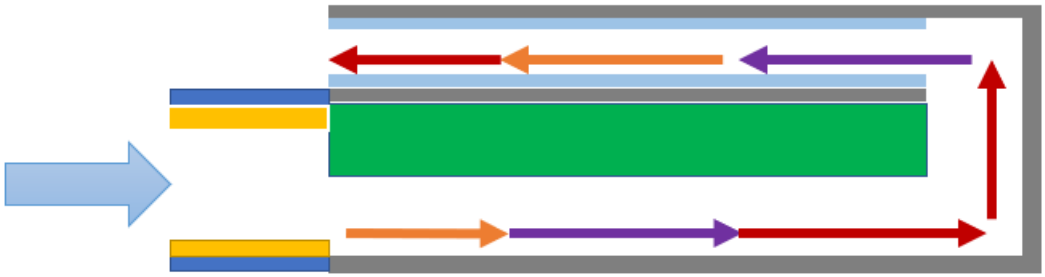

figure 24. Closed M-cycle cooling box with air pretreatment module

The dark part is the shell of dehumidification device, and the yellow part is dehumidification material. The light blue arrow indicates the air entry direction.

On the other hand, as we all know, the interior space of the car is extremely limited, which leads to the strict size limitation of any parts put into the car. The air inlet direction of the M-cycle cooling box is preferably towards the driving direction, so that when the car starts, the wind speed will increase instantly. According to the previous conclusion, the wind speed will also determine the cooling capacity of the system. How to limit the volume, so that it can exert its maximum refrigeration capacity in a limited space, will also be one of the important topics in the future.

References

[1] Lin, J., Thu, K., Bui, T.D., Wang, R.Z., Ng, K.C., Chua, K.J. “Study on dew point evaporative cooling system with counter-flow configuration” (2016) *Energy Conversion and Management*, 109, pp. 153-165.

[2] Sajjad, U., Abbas, N., Hamid, K., (...), Rehman, T.U., Wang, C.C. ‘A review of recent advances in indirect evaporative cooling technolog’ （2021）International Communications in Heat and Mass Transfer

[3] Jain, S., Dhar, P.L., Kaushik, S.C. “Evaluation of solid-desiccant-based evaporative cooling cycles for typical hot and humid climates” （1995）, International Journal of Refrigeration 18(5), pp. 287-296

[4] Z. Duan, Investigation of a Novel Dew Point Indirect Evaporative Air Conditioning System for Buildings, University of Nottingham, 2011.

[5] C.K. Jon, M.R. Islam, N.K. Choon, M.W. Shahzad, Dew-point evaporative cooling systems, in: Advances in Air Conditioning Technologies, Springer, 2020, pp. 53–130.

[6] O. Amer, R. Boukhanouf, H. Ibrahim, A review of evaporative cooling technologies, Int. J. Environ. Sci. Develop. 6 (2) (2015) 111.

[7] S. Delfani, J. Esmaeelian, H. Pasdarshahri, M. Karami, Energy saving potential of an indirect evaporative cooler as a pre-cooling unit for mechanical cooling systems in Iran, Energy and Buildings 42 (11) (2010) 2169–2176.

[8] H.M. Raza, H. Ashraf, K. Shahzad, M. Sultan, T. Miyazaki, M. Usman, R. R. Shamshiri, Y. Zhou, R. Ahmad, Investigating applicability of evaporative cooling Systems for Thermal Comfort of poultry birds in Pakistan, Appl. Sci. 10 (13) (2020) 4445.

[9] H.M. Raza, M. Sultan, M. Bahrami, A.A. Khan, Experimental investigation of evaporative cooling systems for agricultural storage and livestock airconditioning in Pakistan, in: Building Simulation, Springer, 2020, pp. 1–15.

[10] M. Rampazzo, M. Lionello, A. Beghi, E. Sisti, L. Cecchinato, A static moving boundary modelling approach for simulation of indirect evaporative free cooling systems, Appl. Energy 250 (2019) 1719–1728. [11] S. Kashyap, J. Sarkar, A. Kumar, Exergy, economic, environmental and sustainability analyses of possible regenerative evaporative cooling device topologies, Build. Environ. 180 (2020) 107033.

[12] S.J. Oh, M.W. Shahzad, M. Burhan, W. Chun, C.K. Jon, M. KumJa, K.C. Ng, Approaches to energy efficiency in air conditioning: a comparative study on purge configurations for indirect evaporative cooling, Energy 168 (2019) 505–515.

[13] D. Pandelidis, A. Cichon, ´ A. Pacak, S. Anisimov, P. Drąg, Counter-flow indirect evaporative cooler for heat recovery in the temperate climate, Energy 165 (2018) 877–894.

[14] Y. Chen, H. Yan, Y. Min, Development and optimization of a novel controller for regenerative indirect evaporative cooler, Energy Procedia 158 (2019) 2378–2383.

[15] J.-H. Hao, Q. Chen, X. Li, M.-Q. Zhang, F. Yuan, A new modeling and analysis method of the indirect evaporative heat exchanger based on the heat current perspective, Appl. Therm. Eng. 163 (2019) 114331.

[16] M.K. Shahzad, G.Q. Chaudhary, M. Ali, N.A. Sheikh, M.S. Khalil, T.U. Rashid, Experimental evaluation of a solid desiccant system integrated with cross flow Maisotsenko cycle evaporative cooler, Appl. Therm. Eng. 128 (2018) 1476–1487.

[17] A.Y.T. Al-Zubaydi, G. Hong, Experimental study of a novel water-spraying configuration in indirect evaporative cooling, Appl. Therm. Eng. 151 (2019) 283–293.

[18] A. Sohani, H. Sayyaadi, Thermal comfort based resources consumption and economic analysis of a two-stage direct-indirect evaporative cooler with diverse water to electricity tariff conditions, Energy

Convers. Manag. 172 (2018) 248–264.

[19] D. Meng, J. Lv, Y. Chen, H. Li, X. Ma, Visualized experimental investigation on cross-flow indirect evaporative cooler with condensation, Appl. Therm. Eng. 145 (2018) 165–173.

[20] J. Nie, S. Yuan, L. Fang, Q. Zhang, D. Li, Experimental study on an innovative enthalpy recovery technology based on indirect flash evaporative cooling, Appl. Therm. Eng. 129 (2018) 22–30.

[21] S. De Antonellis, L. Cignatta, C. Facchini, P. Liberati, Effect of heat exchanger plates geometry on performance of an indirect evaporative cooling system, in: Applied Thermal Engineering, 2020, p. 115200. [22] S. Sibanda, T.S. Workneh, Performance evaluation of an indirect air cooling system combined with evaporative cooling, Heliyon 6 (1) (2020), e03286.

[23] P. Kowalski, D. Kwiecien, ´ Evaluation of simple evaporative cooling systems in an industrial building in Poland, J. Building Eng. (2020) 101555.

[24] Q. Liu, C. Guo, X. Ma, Y. You, Y. Li, Experimental study on total heat transfer efficiency evaluation of an indirect evaporative cooler, Appl. Therm. Eng. 115287 (2020).

[25] K. Matsui, K. Thu, T. Miyazaki, A hybrid power cycle using an inverted Brayton cycle with an indirect evaporative device for waste-heat recovery, Appl. Therm. Eng. 170 (2020) 115029.

[26] Pandelidis D, Anisimov S. Numerical analysis of the heat and mass transfer processes in selected M-cycle heat exchangers for the dew point evaporative cooling. Energ Convers Manage 2015;90:62–83.

[27] Riffel DB, Wittstadt U, Schmidt FP, Núñez T, Belo FA, Leite APF, et al. Transient modeling of an adsorber using finned-tube heat exchanger. Int J Heat Mass Transf 2010;53:1473–82.

[28] Namvar R, Ge G, Simonson CJ, Besant RW. Transient heat and moisture transfer characteristics of a liquid-to-air membrane energy exchanger (LAMEE) model verification and extrapolation. Int J Heat Mass Transf 2013;66:757–71.

[29] Lenic K, Trp A, Frankovic B. Transient two-dimensional model of frost formation on a fin-and-tube heat exchanger. Int J Heat Mass Transf 2009;52:22–32.

[30] Hettiarachchi HDM, Golubovic M, Worek WM. The effect of longitudinal heat conduction in cross flow indirect evaporative air coolers. Appl Therm Eng 2007;27:1841–8.

[31] Heidarinejad G, Moshari S. Novel modeling of an indirect evaporative cooling system with cross-flow configuration. Energ Build 2015;92:351–62.

[32] Xu J, Wei Q, Peng S, Yu Y. Error of saturation vapor pressure calculated by different formulas and its effect on calculation of reference evapotranspiration in high latitude cold region. Procedia Eng 2012;28:43–8.

[33] M. Conde Engineering. Thermophysical properties of humid air. Zurich, Switzerland; 2007.

[34] Bergman TL, Incropera FP, Lavine AS. Fundamentals of heat and mass transfer. 7th ed. John Wiley & Sons; 2011.

[25] Baehr HD, Stephan K. Heat and mass transfer. 2nd ed. New York, Berlin: Springer; 2006.

[36] Dowdy J, Karabash N. Experimental determination of heat and mass transfer coefficients in rigid impregnated cellulose evaporative media. ASHRAE Trans 1987;93:382–95.

[37] Camargo J, Ebinuma C, Cardoso S. A mathematical model for direct evaporative cooling air conditioning system. Rev Engenharia Térmica 2009;2.

[38] Heidarinejad G, Khalajzadeh V, Delfani S. Performance analysis of a groundassisted direct evaporative cooling air conditioner. Build Environ 2010;45:2421–9.

[39] Wu JM, Huang X, Zhang H. Theoretical analysis on heat and mass transfer in a direct evaporative cooler. Appl Therm Eng 2009;29:980–4

[40] Luis Perez-Lombard JO, Pout C. A review on buildings energy consumption information. Energy and Buildings 2008;40(3):394e8.

[41] U.S. Department of Energy. Energy information administration. International Energy Outlook; 2006. [42] Key world energy statistics. International Energy Agency; 2006.

[43] Kottek M, Grieser J, Beck C, Rudolf B, Rubel F. World map of the Köppen-Geiger climate classification update. Meteorologische Zeitschrift 2006;15(3):259e63.

[44] Center for International Earth Science Information Network (CIESIN), Columbia University; and Centro Internacional de Agricultura Tropical (CIAT). 2005 Gridded Population of the World Version 3 (GPWv3): Population Density Grids. Palisades, NY: Socioeconomic Data and Applications Center (SEDAC), Columbia University. Available at: http://sedac.ciesin.columbia.edu/gpw (03/2011).

[45] Smith S, Hanby VI, Harpham C. A probabilistic analysis of the future potential of evaporative cooling systems in a temperate climate. Energy and Buildings 2010;43(2e3):507e16.

[46] Al-Marafie AMR, Suri RK, Maheshwari GP. Energy and power management in air-conditioned buildings in Kuwait. Energy 1989;9:557e62.

[47] Maheshwari GP, Al-Ragom F, Suri RK. Energy saving potential of an indirect evaporative cooler. Applied Energy 2001;69:69e76.

[48] Goshayshi HR, Missenden JF, Tozer R. Cooling tower e an energy conservation resource. Applied Thermal Engineering 1999;19:1223e35.

[49] Chen Qun, Yang Kangding, Wang Moran, Pan Ning, Guo Zeng-Yuan. A new approach to analysis and optimization of evaporative cooling system I: theory. Energy 2010;35(6):2448e54.

[50] Chen Qun, Pan Ning, Guo Zeng-Yuan. A new approach to analysis and optimization of evaporative cooling system II: applications. Energy 2011;36(5): 2890e8.

[51] Hsu Shyr Tzer, Lavan Zalman, Worek William M. Optimization of wet-surface heat exchangers. Energy 1989;14(11):757e70. [13] ASHRAE handbook: refrigeration. SI Edition. Atlanta, GA 30329, US: American Society of Heating, Refrigeration and Air-Conditioning Engineers, Inc.; 2006. 41.1-10..

[52] CIBSE Guide B4. Refrigeration and heat rejection. Norwich, UK: Page Bros, (Norwich) Ltd; 2003. 19e42.

[53] CIBSE Knowledge Series. Sustainable low energy cooling: an overview. Plymouth PL6 7PY, UK: Latimer Trend & Co. Ltd; 2005. 15e19.

[54] Zhao X, Yang S, Duan Z, Riffat SB. Feasibility study of a now dew point air conditioning system for China building application. Building and Environment 2009;44:1990e9.

[55] Maisotsenko Valeriy, Gillan Leland E, Heaton Timothy L, Gillan Alan D. Method and plate apparatus for dew point evaporative cooler. United State Patent 6,581,402. June 24, 2003.

[56] Coolerado. CooleradoHMX (heat and mass exchanger) brochure. Arvada, Colorado, USA: Coolerado Corporation; 2006.

[57] ISAW. Natural air conditioner (heat and mass exchanger) catalogues. Hangzhou, China: ISAW Corporation Ltd; 2005.

[58] Zhao X, Li JM, Riffat SB. Numerical study of a novel counter-flow heat and mass exchanger for dew point evaporative cooling. Applied Thermal Engineering 2008;28:1942e51.

[59] Zhan C, Zhao X, Smith S, Riffat SB. Numerical study of a M-cycle cross-flow heat exchanger for indirect evaporative cooling. Building and Environment 2011;46:657e68.

[60] Zhao X, Liu S, Riffat SB. Comparative study of heat and mass exchanging materials for indirect evaporative cooling systems. Building and Environment 2008;43:1902e10.

[61] Welty JR, Wicks CE, Wilson RE, Rorrer G. Fundamentals of momentum, heat, and mass transfer, vol. 500e589. USA: John Wiley & Sons Inc; 2000. 288e326.

[62] John H, Lienhard V. A heat transfer textbook. Cambridge, Massachusetts: Phlogiston Press; 2001. 352. [63] Bejan A, Kraus AD. Heat transfer handbook. Hoboken, New Jersey: John Wiley & Sons, Inc.; 2003. 403 and 429e430.

[64] Holman JP. Heat transfer. 9th ed. New York: McGraw-Hill Companies, Inc.; 2002. 273.

[65] CIBSE guide B2. Ventilation and air conditioning, vol. 5. Norwich, UK: Page Bros (Norwich) Ltd; 2001. 25 e 5:28.

[66] Qiu G. A novel evaporative/desiccant cooling system. Dissertation for the degree of Doctor of Philosophy, The University of Nottingham. 2007; 41e60.

[67] Riangvilaikul B, Kumar S. An experimental study of a novel dew point evaporative cooling system. Energy and Buildings 2010;42:637e44.

[68] Duan Z. Investigation of a novel dew point cooling system for building air conditioning. PhD

thesis, University of Nottingham, UK. 2011; pp. 150e180.

[69] Alonso JFSJ, Martinez FJR, Gomez EV, Plasencia MAAG. Simulation model of an indirect evaporative cooler. Energy and Buildings 1998;29:23e7.

[70] Wu M, Huang X, Zhang H. Numerical investigation on the heat and mass transfer in a direct evaporative cooler. Applied Thermal Engineering 2009;29: 195e201.

Acknowledgement

My deepest gratitude is to my supervisors, Professor Takahiko Miyazaki, Associate Professor Kyaw Thu of Energy and Environmental Engineering, IGSES at Kyushu University, for their invaluable and indispensable guidance.

At the initial stage of research, I have no idea about doing research. I am grateful to the two teachers for their guidance at the beginning of the research. It was two professors who taught me how to search papers, how to prepare for the upcoming research, record problems and solve problems. Thank you, Professor Miyazaki, for your tolerance and understanding when I was in trouble, and thank you for answering my various questions by email again and again.

On the topic selection, I thank Marco Lao Reyes for his advice. On the initial topic selection, without Marco, I would have no way to start.

In terms of software learning, I still want to thank Professor Miyazaki for the M-cycle program written by MATLAB earlier, which gave me a reference when I started learning MATLAB.

I would like to thank Chen haonan and Yang cheng for their professional advice and support during my master's study.

Thanks to Yu hao for his support and valuable advice during the research.

Thanks to Sagar Saren for his help in some software application problems.

Thanks to my college classmate Zhu for his support when I was learning to use MATLAB.

Last but not least, I thank my parents for their support during my master's study, both mentally and financially. Thank you for your encouragement during my study.

Appendix A

Saturation Properties for Steam - Temperature Table (0.01°C - 150°C)

Temp	Pressure	volume (m^3/kg)		energy (kJ/kg)		enthalpy (kJ/kg)			entropy (kJ/kg.K)		
°C	MPa	vf	vg	uf	ug	hf	hfg	hg	sf	sfg	sg
0.01	0.00061	0.00100	205.99	0	2374.9	0.001	2500.9	2500.9	0	9.1555	9.1555
5	0.00087	0.00100	147.01	21.02	2381.8	21.0	2489.1	2510.1	0.0763	8.9485	9.0248
10	0.00123	0.00100	106.30	42.02	2388.6	42.0	2477.2	2519.2	0.1511	8.7487	8.8998
15	0.00171	0.00100	77.875	62.98	2395.5	63.0	2465.3	2528.3	0.2245	8.5558	8.7803
20	0.00234	0.00100	57.757	83.91	2402.3	83.9	2453.5	2537.4	0.2965	8.3695	8.6660
25	0.00317	0.00100	43.337	104.83	2409.1	104.8	2441.7	2546.5	0.3672	8.1894	8.5566
30	0.00425	0.00100	32.878	125.73	2415.9	125.7	2429.8	2555.5	0.4368	8.0152	8.4520
35	0.00563	0.00101	25.205	146.63	2422.7	146.6	2417.9	2564.5	0.5051	7.8466	8.3517
40	0.00739	0.00101	19.515	167.53	2429.4	167.5	2406.0	2573.5	0.5724	7.6831	8.2555
45	0.00960	0.00101	15.252	188.43	2436.1	188.4	2394.0	2582.4	0.6386	7.5247	8.1633
50	0.01235	0.00101	12.027	209.33	2442.7	209.3	2382.0	2591.3	0.7038	7.3710	8.0748
55	0.01576	0.00102	9.5643	230.24	2449.3	230.3	2369.8	2600.1	0.7680	7.2218	7.9898
60	0.01995	0.00102	7.6672	251.16	2455.9	251.2	2357.6	2608.8	0.8313	7.0768	7.9081
65	0.02504	0.00102	6.1935	272.09	2462.4	272.1	2345.4	2617.5	0.8937	6.9359	7.8296
70	0.03120	0.00102	5.0395	293.03	2468.9	293.2	2333.0	2626.1	0.9551	6.7989	7.7540
75	0.03860	0.00103	4.1289	313.99	2475.2	314.0	2320.6	2634.6	1.0158	6.6654	7.6812
80	0.04741	0.00103	3.4052	334.96	2481.6	335.0	2308.0	2643.0	1.0756	6.5355	7.6111
85	0.05787	0.00103	2.8258	355.95	2487.8	356.0	2295.3	2651.3	1.1346	6.4088	7.5434
90	0.07018	0.00104	2.3591	376.97	2494.0	377.0	2282.5	2659.5	1.1929	6.2852	7.4781
95	0.08461	0.00104	1.9806	398.00	2500.0	398.1	2269.5	2667.6	1.2504	6.1647	7.4151
100	0.10142	0.00104	1.6718	419.06	2506.0	419.2	2256.4	2675.6	1.3072	6.0469	7.3541
110	0.14338	0.00105	1.2093	461.26	2517.7	461.4	2229.7	2691.1	1.4188	5.8193	7.2381
120	0.19867	0.00106	0.8912	503.60	2528.9	503.8	2202.1	2705.9	1.5279	5.6012	7.1291
130	0.27028	0.00107	0.66800	546.09	2539.5	546.4	2173.7	2720.1	1.6346	5.3918	7.0264
140	0.36154	0.00108	0.50845	588.77	2549.6	589.2	2144.2	2733.4	1.7392	5.1901	6.9293
150	0.47616	0.00109	0.39245	631.66	2559.1	632.2	2113.7	2745.9	1.8418	4.9953	6.8371

Appendix B

```
clear;
channel_len = 0.95;      % len of channel, meter    0.1~0.12
channel_width = 0.09; % width of channel, meter
channel_height_dry = 0.005;    % meter
channel_height_wet = 0.0025; % meter
m = 2.63;                    % kg, weight of battery
cp = 880;                    % Specific heat capacity of battery
v_air = 3;                   % m/s
temp_room = 27;              % centigrade
h_water = 1399000;           % J/kg
h_vapour= 2550000;           % J/kg
p = 0.101;                   % air pressure, MPa
rou = 1.29;                  %Density of air, kg/m^3
lambda =    237;             % w/mk, Thermal conductivity of battery
I = 138;                     % current
R = 1.8e-3;                  % battery resistence

WATER_TEMP =[7,18,26,30,35,40,45,50,55,60,65,70,75,80,85];
% steam pressure, MPa
PS = [0.001,0.002,0.003,0.004,0.005,0.007,0.009,0.012,0.015,0.019,0.025,0.031,0,038,0.047,0.057];
TEMP = [-50, -40, -30, -20, -10, 0, 10, 20, 30, 40,50,60,70,80,90,100, 120, 140, 160,180, 200, 250,
300, 350, 400, 500, 600, 700,800, 900, 1000, 1100, 1200];
PR = [0.728, 0.728, 0.723, 0.716, 0.712, 0.707, 0.705, 0.703,0.701, 0.699, 0.698, 0.696, 0.694, 0.692,
0.690, 0.688,0.686,0.684, 0.682, 0.681, 0.680, 0.677, 0.674, 0.676, 0.678, 0.687, 0.699, 0.706, 0.713,
0.717, 0.719, 0.722, 0.724];
% Aerodynamic viscosity
V_AV = [9.23, 10.04, 10.80, 11.61, 12.43, 13.28, 14.16, 15.06, 16.00 16.96, 17.95, 18.97, 20.02,
21.09, 22.10, 23.13, 25.45, 27.80, 30.09, 32.49, 34.85, 40.61, 48.33, 55.46, 63.09, 79.38, 96.89, 115.4,
134.8, 155.1, 177.1, 199.3, 233.7];

deltat = 1;
temp_battery = temp_room; % initial battery tempurary is equal to room
channel_width = 0.05; % width of channel, meter
temp_curve=1:3600*2;
```

```
for i=1:length(temp_curve)
    Pr = PR(1);
    v_av = V_AV(1);
    for t = 1:length(TEMP)-10
        if temp_battery>TEMP(t)
            Pr = PR(t);
            v_av = V_AV(t);
        else
            break;
        end
    end
    Re = v_air*channel_len/v_av;
    Nn = 0.664*(Re^(1/2))*(Pr^(1/3));
    h = lambda/channel_len*Nn;
    temp_wet_in = temp_room+h*(channel_len*channel_width)*(temp_battery-temp_room)/cp;
    ps = PS(1);
    for t = 1:length(WATER_TEMP)
        if temp_battery>TEMP(t)
            ps = PS(t);
        else
            break;
        end
    end

    d_wet_out = 0.622*ps/(p-ps);
    d_wet_in = 0.622*0.4*ps/(p-0.4*ps);
    wet_channel = rou*channel_len*channel_width*channel_height_wet*(h_vapour -
h_water)*(d_wet_out-d_wet_in);
    temp_battery = temp_battery+(I^2*R-h*(channel_len*channel_width)*(temp_battery-
temp_room)-wet_channel)*deltat/m/cp;
    temp_curve(i)=temp_battery;
end

temp_battery = temp_room; % initial battery tempurary is equal to room
channel_width = 0.08; % width of channel, meter
temp_curve2=1:3600*2;
for i=1:length(temp_curve2)
```

```
    Pr = PR(1);
    v_av = V_AV(1);
    for t = 1:length(TEMP)-10
        if temp_battery>TEMP(t)
            Pr = PR(t);
            v_av = V_AV(t);
        else
            break;
        end
    end
    Re = v_air*channel_len/v_av;
    Nn = 0.664*(Re^(1/2))*(Pr^(1/3));
    h = lambda/channel_len*Nn;
    temp_wet_in = temp_room+h*(channel_len*channel_width)*(temp_battery-temp_room)/cp;
    ps = PS(1);
    for t = 1:length(WATER_TEMP)
        if temp_battery>TEMP(t)
            ps = PS(t);
        else
            break;
        end
    end

    d_wet_out = 0.622*ps/(p-ps);
    d_wet_in = 0.622*0.4*ps/(p-0.4*ps);
    wet_channel = rou*channel_len*channel_width*channel_height_wet*(h_vapour -
h_water)*(d_wet_out-d_wet_in);
    temp_battery = temp_battery+(I^2*R-h*(channel_len*channel_width)*(temp_battery-
temp_room)-wet_channel)*deltat/m/cp;
    temp_curve2(i)=temp_battery;
end

temp_battery = temp_room; % initial battery tempurary is equal to room
channel_width = 0.1; % width of channel, meter
temp_curve3=1:3600*2;
for i=1:length(temp_curve3)
    Pr = PR(1);
```

```
    v_av = V_AV(1);
    for t = 1:length(TEMP)-10
        if temp_battery>TEMP(t)
            Pr = PR(t);
            v_av = V_AV(t);
        else
            break;
        end
    end
    Re = v_air*channel_len/v_av;
    Nn = 0.664*(Re^(1/2))*(Pr^(1/3));
    h = lambda/channel_len*Nn;
    temp_wet_in = temp_room+h*(channel_len*channel_width)*(temp_battery-temp_room)/cp;
    ps = PS(1);
    for t = 1:length(WATER_TEMP)
        if temp_battery>TEMP(t)
            ps = PS(t);
        else
            break;
        end
    end

    d_wet_out = 0.622*ps/(p-ps);
    d_wet_in = 0.622*0.4*ps/(p-0.4*ps);
    wet_channel = rou*channel_len*channel_width*channel_height_wet*(h_vapour -
h_water)*(d_wet_out-d_wet_in);
    temp_battery = temp_battery+(I^2*R-h*(channel_len*channel_width)*(temp_battery-
temp_room)-wet_channel)*deltat/m/cp;
    temp_curve3(i)=temp_battery;
end

figure('Position',[100 100 1100 500]);
h=plot(1:length(temp_curve),temp_curve);
hold on;
h=[h,plot(1:length(temp_curve2),temp_curve2);]
h=[h,plot(1:length(temp_curve3),temp_curve3);]
h=[h,scatter(2500,33.8)];
```

```
text(2500-350,33.8+0.2,'2500 / 33.8')
h=[h,scatter(800,30.05)];
text(800-350,30.05+0.2,'800 / 30.05')
h=[h,scatter(1000,29.15)];
text(1000-350,29.15+0.2,'1000 / 29.15')

legend(h([1,2,3]),'width:5mm','width:8mm','width:10mm');
xlabel('time:seconds');
ylabel('battery temperature');
title('battery simulation');

temp_battery = temp_room; % initial battery tempurary is equal to room
channel_width = 0.05; % width of channel, meter
v_air = 5;                    % m/s
temp_curve4=1:3600*2;
for i=1:length(temp_curve4)
    Pr = PR(1);
    v_av = V_AV(1);
    for t = 1:length(TEMP)-10
        if temp_battery>TEMP(t)
            Pr = PR(t);
            v_av = V_AV(t);
        else
            break;
        end
    end
    Re = v_air*channel_len/v_av;
    Nn = 0.664*(Re^(1/2))*(Pr^(1/3));
    h = lambda/channel_len*Nn;
    temp_wet_in = temp_room+h*(channel_len*channel_width)*(temp_battery-temp_room)/cp;
    ps = PS(1);
    for t = 1:length(WATER_TEMP)
        if temp_battery>TEMP(t)
            ps = PS(t);
        else
            break;
        end
```

```
    end

    d_wet_out = 0.622*ps/(p-ps);
    d_wet_in = 0.622*0.4*ps/(p-0.4*ps);
    wet_channel = rou*channel_len*channel_width*channel_height_wet*(h_vapour -
h_water)*(d_wet_out-d_wet_in);
    temp_battery = temp_battery+(I^2*R-h*(channel_len*channel_width)*(temp_battery-
temp_room)-wet_channel)*deltat/m/cp;
    temp_curve4(i)=temp_battery;
end


temp_battery = temp_room; % initial battery tempurary is equal to room
v_air = 20;                 % m/s
temp_curve5=1:3600*2;
for i=1:length(temp_curve5)
    Pr = PR(1);
    v_av = V_AV(1);
    for t = 1:length(TEMP)-10
        if temp_battery>TEMP(t)
            Pr = PR(t);
            v_av = V_AV(t);
        else
            break;
        end
    end
    Re = v_air*channel_len/v_av;
    Nn = 0.664*(Re^(1/2))*(Pr^(1/3));
    h = lambda/channel_len*Nn;
    temp_wet_in = temp_room+h*(channel_len*channel_width)*(temp_battery-temp_room)/cp;
    ps = PS(1);
    for t = 1:length(WATER_TEMP)
        if temp_battery>TEMP(t)
            ps = PS(t);
        else
            break;
        end
```

```
    end

    d_wet_out = 0.622*ps/(p-ps);
    d_wet_in = 0.622*0.4*ps/(p-0.4*ps);
    wet_channel = rou*channel_len*channel_width*channel_height_wet*(h_vapour -
h_water)*(d_wet_out-d_wet_in);
    temp_battery = temp_battery+(I^2*R-h*(channel_len*channel_width)*(temp_battery-
temp_room)-wet_channel)*deltat/m/cp;
    temp_curve5(i)=temp_battery;
end

temp_battery = temp_room; % initial battery tempurary is equal to room
v_air = 50;                 % m/s
temp_curve6=1:3600*2;
for i=1:length(temp_curve6)
    Pr = PR(1);
    v_av = V_AV(1);
    for t = 1:length(TEMP)-10
        if temp_battery>TEMP(t)
            Pr = PR(t);
            v_av = V_AV(t);
        else
            break;
        end
    end
    Re = v_air*channel_len/v_av;
    Nn = 0.664*(Re^(1/2))*(Pr^(1/3));
    h = lambda/channel_len*Nn;
    temp_wet_in = temp_room+h*(channel_len*channel_width)*(temp_battery-temp_room)/cp;
    ps = PS(1);
    for t = 1:length(WATER_TEMP)
        if temp_battery>TEMP(t)
            ps = PS(t);
        else
            break;
        end
    end
```

```
        d_wet_out = 0.622*ps/(p-ps);
        d_wet_in = 0.622*0.4*ps/(p-0.4*ps);
        wet_channel = rou*channel_len*channel_width*channel_height_wet*(h_vapour -
h_water)*(d_wet_out-d_wet_in);
        temp_battery = temp_battery+(I^2*R-h*(channel_len*channel_width)*(temp_battery-
temp_room)-wet_channel)*deltat/m/cp;
        temp_curve6(i)=temp_battery;
end

figure('Position',[120 120 1100 500]);
plot(1:length(temp_curve4),temp_curve4,1:length(temp_curve5),temp_curve5,1:length(temp_curve6),
temp_curve6);
legend('air-speed:5','air-speed:20','air-speed:50');
xlabel('time:seconds');
ylabel('battery temperature');
title('battery simulation');

temp_battery = temp_room; % initial battery tempurary is equal to room
v_air = 5;                    % m/s
I = 27;                       % current
temp_curve7=1:3600*2;
for i=1:length(temp_curve7)
        Pr = PR(1);
        v_av = V_AV(1);
        for t = 1:length(TEMP)-10
                if temp_battery>TEMP(t)
                        Pr = PR(t);
                        v_av = V_AV(t);
                else
                        break;
                end
        end
        Re = v_air*channel_len/v_av;
        Nn = 0.664*(Re^(1/2))*(Pr^(1/3));
        h = lambda/channel_len*Nn;
        temp_wet_in = temp_room+h*(channel_len*channel_width)*(temp_battery-temp_room)/cp;
```

```
    ps = PS(1);
    for t = 1:length(WATER_TEMP)
        if temp_battery>TEMP(t)
            ps = PS(t);
        else
            break;
        end
    end

    d_wet_out = 0.622*ps/(p-ps);
    d_wet_in = 0.622*0.4*ps/(p-0.4*ps);
    wet_channel = rou*channel_len*channel_width*channel_height_wet*(h_vapour -
h_water)*(d_wet_out-d_wet_in);
    temp_battery = temp_battery+(I^2*R-h*(channel_len*channel_width)*(temp_battery-
temp_room)-wet_channel)*deltat/m/cp;
    temp_curve7(i)=temp_battery;
end

temp_battery = temp_room; % initial battery tempurary is equal to room
I = 138;                  % current
temp_curve8=1:3600*2;
for i=1:length(temp_curve8)
    Pr = PR(1);
    v_av = V_AV(1);
    for t = 1:length(TEMP)-10
        if temp_battery>TEMP(t)
            Pr = PR(t);
            v_av = V_AV(t);
        else
            break;
        end
    end
    Re = v_air*channel_len/v_av;
    Nn = 0.664*(Re^(1/2))*(Pr^(1/3));
    h = lambda/channel_len*Nn;
    temp_wet_in = temp_room+h*(channel_len*channel_width)*(temp_battery-temp_room)/cp;
    ps = PS(1);
```

```
    for t = 1:length(WATER_TEMP)
        if temp_battery>TEMP(t)
            ps = PS(t);
        else
            break;
        end
    end

    d_wet_out = 0.622*ps/(p-ps);
    d_wet_in = 0.622*0.4*ps/(p-0.4*ps);
    wet_channel = rou*channel_len*channel_width*channel_height_wet*(h_vapour -
h_water)*(d_wet_out-d_wet_in);
    temp_battery = temp_battery+(I^2*R-h*(channel_len*channel_width)*(temp_battery-
temp_room)-wet_channel)*deltat/m/cp;
    temp_curve8(i)=temp_battery;
end

temp_battery = temp_room; % initial battery tempurary is equal to room
I = 200;                          % current
temp_curve9=1:3600*2;
for i=1:length(temp_curve9)
    Pr = PR(1);
    v_av = V_AV(1);
    for t = 1:length(TEMP)-10
        if temp_battery>TEMP(t)
            Pr = PR(t);
            v_av = V_AV(t);
        else
            break;
        end
    end
    Re = v_air*channel_len/v_av;
    Nn = 0.664*(Re^(1/2))*(Pr^(1/3));
    h = lambda/channel_len*Nn;
    temp_wet_in = temp_room+h*(channel_len*channel_width)*(temp_battery-temp_room)/cp;
    ps = PS(1);
    for t = 1:length(WATER_TEMP)
```

```
        if temp_battery>TEMP(t)
            ps = PS(t);
        else
            break;
        end
    end

    d_wet_out = 0.622*ps/(p-ps);
    d_wet_in = 0.622*0.4*ps/(p-0.4*ps);
    wet_channel = rou*channel_len*channel_width*channel_height_wet*(h_vapour -
h_water)*(d_wet_out-d_wet_in);
    temp_battery = temp_battery+(I^2*R-h*(channel_len*channel_width)*(temp_battery-
temp_room)-wet_channel)*deltat/m/cp;
    temp_curve9(i)=temp_battery;
end


figure('Position',[130 130 1100 500]);
plot(1:length(temp_curve7),temp_curve7,1:length(temp_curve8),temp_curve8,1:length(temp_curve9),
temp_curve9);
legend('current:27','current:138','current:200');
xlabel('time:seconds');
ylabel('battery temperature');
title('battery simulation');

temp_battery = temp_room; % initial battery tempurary is equal to room
v_air = 5;                  % m/s
I = 138;                    % current
channel_height_wet = 0.0025; % meter
temp_curve10=1:3600*2;
for i=1:length(temp_curve10)
    Pr = PR(1);
    v_av = V_AV(1);
    for t = 1:length(TEMP)-10
        if temp_battery>TEMP(t)
            Pr = PR(t);
            v_av = V_AV(t);
```

```
        else
            break;
        end
    end
    Re = v_air*channel_len/v_av;
    Nn = 0.664*(Re^(1/2))*(Pr^(1/3));
    h = lambda/channel_len*Nn;
    temp_wet_in = temp_room+h*(channel_len*channel_width)*(temp_battery-temp_room)/cp;
    ps = PS(1);
    for t = 1:length(WATER_TEMP)
        if temp_battery>TEMP(t)
            ps = PS(t);
        else
            break;
        end
    end

    d_wet_out = 0.622*ps/(p-ps);
    d_wet_in = 0.622*0.4*ps/(p-0.4*ps);
    wet_channel = rou*channel_len*channel_width*channel_height_wet*(h_vapour -
h_water)*(d_wet_out-d_wet_in);
    temp_battery = temp_battery+(I^2*R-h*(channel_len*channel_width)*(temp_battery-
temp_room)-wet_channel)*deltat/m/cp;
    temp_curve10(i)=temp_battery;
end

temp_battery = temp_room; % initial battery tempurary is equal to room
channel_height_wet = 0.003; % meter
temp_curve11=1:3600*2;
for i=1:length(temp_curve11)
    Pr = PR(1);
    v_av = V_AV(1);
    for t = 1:length(TEMP)-10
        if temp_battery>TEMP(t)
            Pr = PR(t);
            v_av = V_AV(t);
        else
```

```
            break;
        end
    end
    Re = v_air*channel_len/v_av;
    Nn = 0.664*(Re^(1/2))*(Pr^(1/3));
    h = lambda/channel_len*Nn;
    temp_wet_in = temp_room+h*(channel_len*channel_width)*(temp_battery-temp_room)/cp;
    ps = PS(1);
    for t = 1:length(WATER_TEMP)
        if temp_battery>TEMP(t)
            ps = PS(t);
        else
            break;
        end
    end

    d_wet_out = 0.622*ps/(p-ps);
    d_wet_in = 0.622*0.4*ps/(p-0.4*ps);
    wet_channel = rou*channel_len*channel_width*channel_height_wet*(h_vapour -
h_water)*(d_wet_out-d_wet_in);
    temp_battery = temp_battery+(I^2*R-h*(channel_len*channel_width)*(temp_battery-
temp_room)-wet_channel)*deltat/m/cp;
    temp_curve11(i)=temp_battery;
end

temp_battery = temp_room; % initial battery tempurary is equal to room
channel_height_wet = 0.005; % meter
temp_curve12=1:3600*2;
for i=1:length(temp_curve12)
    Pr = PR(1);
    v_av = V_AV(1);
    for t = 1:length(TEMP)-10
        if temp_battery>TEMP(t)
            Pr = PR(t);
            v_av = V_AV(t);
        else
            break;
```

```
        end
    end
    Re = v_air*channel_len/v_av;
    Nn = 0.664*(Re^(1/2))*(Pr^(1/3));
    h = lambda/channel_len*Nn;
    temp_wet_in = temp_room+h*(channel_len*channel_width)*(temp_battery-temp_room)/cp;
    ps = PS(1);
    for t = 1:length(WATER_TEMP)
        if temp_battery>TEMP(t)
            ps = PS(t);
        else
            break;
        end
    end

    d_wet_out = 0.622*ps/(p-ps);
    d_wet_in = 0.622*0.4*ps/(p-0.4*ps);
    wet_channel = rou*channel_len*channel_width*channel_height_wet*(h_vapour -
h_water)*(d_wet_out-d_wet_in);
    temp_battery = temp_battery+(I^2*R-h*(channel_len*channel_width)*(temp_battery-
temp_room)-wet_channel)*deltat/m/cp;
    temp_curve12(i)=temp_battery;
end


figure('Position',[140 140 1100 500]);
plot(1:length(temp_curve10),temp_curve10,1:length(temp_curve11),temp_curve11,1:length(temp_cur
ve12),temp_curve12);
legend('wet-channel height:2.5mm','wet-channel height:3mm','wet-channel height:5mm');
xlabel('time:seconds');
ylabel('battery temperature');
title('battery simulation');
```